IEEE Open Journal of
Intelligent Transportation
Systems

Received 20 November 2025; revised 13 February 2026; accepted 7 March 2026. Date of publication 10 March 2026; date of current version 17 March 2026.

Digital Object Identifier 10.1109/OJITS.2026.3672438

A Vehicle-in-the-Loop Approach for Front Camera Verification Using Adaptive High Beam

ROBIN LANGER[1], THOMAS TENTRUP[2], AND HANS-GEORG SCHWEIGER[1] (Member, IEEE)

[1]CARISSMA Institute of Electric, Connected and Secure Mobility (C-ECOS), Technische Hochschule Ingolstadt, 85049 Ingolstadt, Germany
[2]KÜS Bundesgeschäftsstelle, 66679 Losheim am See, Germany

CORRESPONDING AUTHOR: R. LANGER (Robin.Langer@thi.de)

This work was supported in part by the Bundesministerium für Bildung und Forschung (BMBF) Fachhochschule (FH)-Impuls 2020 Safety for all – Innovative Research Partnership on Global Vehicle and Road Safety Systems (SAFIR) Automatisierte und vernetzte Elektrofahrzeuge vor, während und nach einem Unfall (AVENUE) under Grant 13FH7I05IA and in part by the Open Access Publication Fund of Technische Hochschule Ingolstadt (THI).

ABSTRACT As automated driving functions based on environmental sensors become increasingly deployed, ensuring reliable performance over the vehicle lifetime is essential. Currently, verification is carried out through internal self-diagnostics, which do not always operate correctly, and periodic technical inspection, which assesses only the test criteria *installation* and *condition*. Test criteria for *function* and *efficiency* of environmental sensors are neither standardized nor routinely assessed, creating the need for new testing approaches. Previous low-cost research approaches defined a method and conducted experiments to verify a vehicle's front camera by displaying visual stimuli and evaluating the high beam assist response. Whereas the camera's *function* could be verified through a basic qualitative check, the approach did not enable a quantitative evaluation of its performance. The aim of this work was therefore to advance this approach and investigate the added value of a Vehicle-in-the-Loop test bench for front camera verification. Three tests were conducted. A supporting method was introduced to reproducibly detect and define the position of the headlight cutoff line, enabling consistent evaluation of the vehicle's reaction. With static camera stimuli (Test I), the *function* of the front camera could be verified, and the influence of the vehicle geometry on the reaction was assessed. Dynamic stimuli (Test II) additionally enabled an *efficiency* evaluation, allowing quantitative comparison between vehicles. However, transferring the stimuli into a reproducible virtual simulation (Test III) remained challenging, as the vehicles under test did not respond consistently. Further research is required to refine and simplify the method toward a standardized periodic technical inspection procedure.

INDEX TERMS Advanced driver assistance systems, automated vehicle, automotive environment detection, camera calibration, inspection, intelligent vehicle, lighting, reliability testing, road vehicle testing, safety.

I. INTRODUCTION

WITH the increasing deployment of automated driving functions [1], [2], [3], the reliable performance of environmental sensors is crucial for safe operation over the vehicle's lifetime. Regulation (EU) 2019/2144 [4] mandates the installation of several driver assistance systems in all new vehicle types from July 2022 and in all new registrations from July 2024. Environmental sensor data form the basis for perceiving the environment and thus for implementing driving functions and safety-critical reactions. To ensure road safety, the performance must remain reliable after years of operation.

Besides numerous model-based approaches [5], [6], [7], [8], [9], environmental sensors can also be assessed *in-use* on the vehicle under real operating conditions, e.g., through onboard self-diagnostics, service procedures (where available), or Periodic Technical Inspections (PTI) to monitor their operational capability over the vehicle lifetime.

The vehicle manufacturer continuously runs vehicle self-diagnostics. However, studies show that even significant or deliberately induced faults are not always detected, highlighting the need for complementary verification methods [10], [11]. In addition, the exact operation and composition of these systems are not transparent to independent third parties because Original Equipment Manufacturers (OEMs) do not disclose this information.

Service work is conducted when the customer brings the vehicle in, for example, at manufacturer-defined intervals, or in response to fault indications. In service, a vehicle's fault memory is often read to retrieve Diagnostic Trouble Codes (DTCs), which indicate potential system malfunctions. There is no regular verification of the environmental sensors in this

The review of this article was arranged by Associate Editor Jianwu Fang.

process. On the contrary, repairs can significantly affect the performance of automated driving functions [12]. For example, after a windshield replacement, the front camera must be correctly aligned and verified to ensure full performance.

PTI provides regular verification of a vehicle's safety, roadworthiness, and environmental compliance. In Germany, it is governed by Directive 2014/45/EU [13], the Road Traffic Registration Ordinance (StVZO) [14], and related national regulations. For passenger cars of vehicle class M1 that are not used as taxis or rental vehicles, the first PTI is required after three years, and subsequent inspections are required every two years. For other vehicle categories or special applications, different intervals may apply as specified in the StVZO [14]. The inspection must be non-destructive and performed without removing any components [14]. The FSD Fahrzeugsystemdaten GmbH (FSD) [15] serves as Germany's designated Central Agency for PTI on behalf of the Federal Republic of Germany and issues binding technical guidelines and inspection instructions for the PTI process. PTI may only be carried out by officially authorized inspectors, typically from organizations such as KÜS [16], TÜV SÜD [17], DEKRA [18], or GTÜ [19]. In Germany, PTI inspectors undergo a dedicated qualification pathway and typically have an academic technical background in addition to the formal authorization requirements. The PTI outcome depends on the severity of detected deficiencies (e.g., none, minor, major, or dangerous). Importantly, PTI inspectors generally do not perform repairs during the inspection; instead, any required corrective actions are carried out subsequently, typically in a workshop. While other works explicitly investigate specific camera fault types [20], [21], the primary objective of PTI is not to diagnose the exact root cause or prescribe a repair procedure, but to determine whether deficiencies are present that affect roadworthiness and therefore require remediation.

The technical assessment during PTI is based on four test criteria [14], which are illustrated and exemplified here using a front camera:

- **Installation:** Is the camera present as required and correctly mounted?
- **Condition:** Is the camera externally intact and operable (e.g., no dirt or damage on the lens or windshield)?
- **Function:** Does the electronic control unit detect and basically process a camera signal?
- **Efficiency:** How reproducibly and to what extent can the camera's performance be measured and evaluated?

As analyzed in [22], the *installation* and *condition* test criteria of environmental sensors are currently electronically verified via the On-Board Diagnostics (OBD) interface in the PTI, typically using the standardized PTI adapter and guided test workflow provided by the FSD, which leads the inspector through the procedure and outputs corresponding inspection notes. However, standardized test methods for verifying the environmental sensors' *function* and *efficiency* are not consistently covered by the OBD-based PTI routine, may not be accessible via OBD, or are not applied in practice.

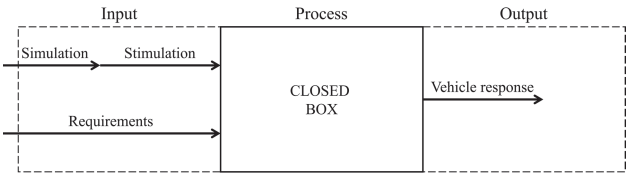

FIGURE 1. Schematic *Input-Process-Output* principle for front camera verification [24].

To explicitly emphasize this point: at present, there are no established PTI procedures that routinely verify the *function* and *efficiency* of vehicle environment sensors or Advanced Driver Assistance Systems (ADAS) in a standardized manner.

Automated driving and environmental sensing introduce complex systems and new challenges for PTI. There is a growing need for adapted and additional methods to verify the performance of safety-critical perception [22], [23]. A key challenge for independent third parties is the lack of intrinsic vehicle knowledge [22]. Only OEMs know the exact system behaviors and dependencies. This makes it significantly more challenging for third parties to develop new test approaches.

Addressing these challenges, [24] developed a generic test method for verifying environmental sensors and demonstrated it using a front camera as an example. The aim was to develop a method for verifying camera performance independently of OEM. The approach follows an *Input-Process-Output* principle (see Fig. 1), which has also been used as a methodological framework in other work [24], [25].

The method first stimulates the sensor (Input), then the vehicle processes sensor data internally (Process), and finally, a measurable vehicle reaction (Output) is recorded and evaluated. For the front camera, stimulation was used, either projected on a screen in front of the vehicle or displayed directly in front of the camera. Internal processing was treated as a closed box. Deactivation of the high beam through the automatic high beam assist, coupled to the front camera, served as an indicator. The assumption was that a traffic participant in the simulation was correctly recognized by the front camera, causing the high beam assist to deactivate the high beam accordingly. Several technical concepts were developed and evaluated. A promising concept was successfully demonstrated in a proof of concept. [24]

In [25], this approach was extended, and the method was studied in detail for a vehicle front camera. The concept still adheres to the same *Input-Process-Output* principle. Stimulation was performed with a display positioned and covered directly in front of the camera, allowing for reproducible scenes independent of ambient light. The setup is shown in Fig. 2.

A tablet was positioned directly in front of the camera and covered by a box. With the high beam assist active, a simulation was executed on the tablet via a remote device, allowing the vehicle's reaction to be provoked. Various traffic scenarios, display brightness levels, static color images, and CAN data were analyzed to identify relevant triggers and reactions. The results confirmed the general suitability of the

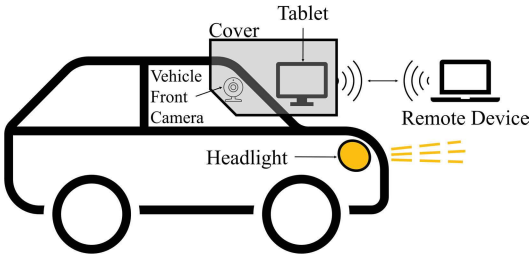

FIGURE 2. Schematic setup in [25]. A tablet positioned directly in front of the camera, covered by a box to protect it from ambient light, is controlled via a remote device to initiate the simulation.

approach. However, they also showed that perceived changes in display brightness often dominated the vehicle's response. Consequently, only a very basic *function* check of the front camera was feasible. In contrast to ViL test benches, this setup represents a low-cost, portable alternative that could, in principle, be deployed in routine PTI facilities with minimal equipment, making it attractive for a basic camera inspection. From a cost perspective, the method is highly attractive, but its practical integration into periodic technical inspection would require significant time optimization to avoid excessive test duration and associated costs.

While there are other test approaches that are generally less costly than a ViL setup, none of them is currently standardized, prescribed, or routinely integrated into PTI, and they are therefore not used in PTI practice today. Examples include stand-alone radar test equipment (e.g., Rohde & Schwarz *RadEsT* [26]) or emerging PTI-supporting robotic concepts (e.g., MAHA *MAIA* [27]). Moreover, the FSD has proposed an approach for ADAS and environmental sensor testing, but it is not yet series-ready and has so far only been demonstrated on a research vehicle with access to sensor raw data; For series vehicles, such an implementation is currently not feasible due to limited third-party access, as raw data from environmental sensors are not available via standardized interfaces [10], [28]. Overall, these approaches range from conceptual prototypes to commercially available products, but they are neither mandated nor established within PTI workflows. In terms of cost, they might be below that of a ViL test bench, yet depending on the concrete implementation they can still be significantly more expensive than the simple front camera *function* test in [24] and [25]. For such single-sensor checks and other low-cost concepts, it remains an open and practically relevant question whether a meaningful integration into PTI is justified, since the cumulative effect of multiple additional checks may substantially increase both investment costs and inspection time. Beyond the setup in this work, other ViL approaches have been proposed to evaluate vehicle environment perception and ADAS under controlled and reproducible conditions such as x-proof-360 from DÜRR [29]. Consequently, it is crucial to clarify which sensor verification procedures will be standardized for PTI in the future and how they can be integrated efficiently.

This work adapts and verifies the previously developed method [24], [25] on a Vehicle-in-the-Loop (ViL) test bench for front camera verification using adaptive high beams. The objective is to obtain both qualitative and quantitative insights for the test criteria *function* and *efficiency* under PTI constraints (e.g., non-destructive testing). The ViL test bench is used as a controlled and highly reproducible environment to fundamentally assess whether the method and the resulting insights are suitable and meaningful under PTI constraints. For an actual PTI deployment, the procedure could subsequently be simplified based on an available standardized interface and a reduced stimulation setup, such that a full ViL system would not be required and the investment costs become more realistic for routine PTI institutions.

In this work, the *function* of the camera is considered fulfilled when a dimming of the adaptive high beam is triggered as a vehicle reaction to the visual stimulation. This indicates that the camera detected the object and responded accordingly. The *efficiency* criterion, in contrast, evaluates how accurately and consistently the vehicle's reaction is performed. For this purpose, a supporting method is introduced, defined as the distance between the detected object position and the transition between a dimmed and a fully illuminated segment—the so-called headlight cutoff line of the adaptive high beam. Three tests were conducted to validate the method.

Test I investigates the suitability of the ViL setup as a proof of concept for verifying the *function* of the front camera through its interaction with the high beam assist. The focus is on the qualitative reaction. It is examined whether a defined stimulus triggers the automatic activation or deactivation of specific segments of the adaptive high beam. Additionally, different orientations of the geometric thrust axis are simulated by modifying the right rear wheel toe within the camera calibration process, without physically changing the actual axle geometry. This represents a realistic scenario, such as a minor curb impact after which the vehicle's axle geometry has not been realigned. The influence of the geometric thrust axis direction on the resulting adaptive high beam segments is analyzed.

Test II extends the approach to a quantitative *efficiency* test. The analysis determines to what extent and how consistently the front camera triggers a correct vehicle reaction when detecting a dynamically moving target.

Test III transfers the *efficiency* test into a highly reproducible simulation-based environment. The evaluation procedure remains identical to Test II, allowing a direct comparison between results obtained with real and simulated stimuli.

The paper is organized as follows. Section II introduces the theoretical background required to understand the subsequent analyses, including adaptive headlight systems, the KÜS DRIVE Vehicle-in-the-Loop test bench, and relevant aspects of vehicle geometry. Section III describes the test design and is structured according to the individual test cases. Section IV presents and discusses the experimental results. Finally, Section V summarizes the main findings of this work.

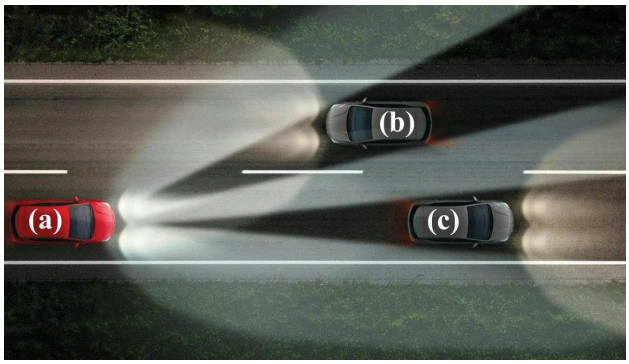

FIGURE 3. Example of a vehicle with the high beam assist activated the adaptive high beam [39]. Vehicle (a) has the adaptive high beam active. The oncoming vehicle (b) and the preceding vehicle (c) are shadowed because the high beam assist deactivated the high beam in these segments. The rest remains illuminated.

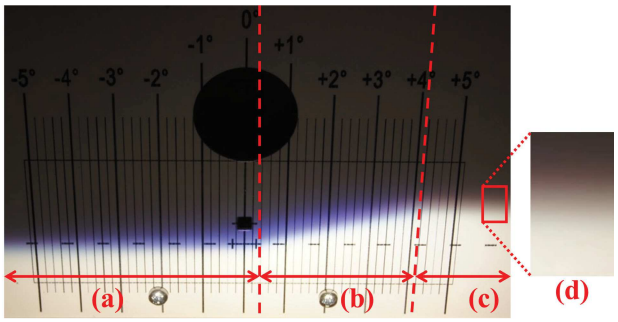

FIGURE 4. Example of a horizontal cutoff line at a beamsetter [40]. The image shows the low beam, the high beam is off. Areas (a), (b), and (c) show different parts of the cutoff line: (a) horizontal, (b) rising to illuminate the roadside better, (c) horizontal again for constant lateral light. Area (d) magnifies the vertical transition from shadowed (top) to illuminated (bottom) for the horizontal cutoff line.

II. THEORETICAL BACKGROUND

A. ADAPTIVE HEADLIGHT SYSTEMS

Modern vehicles can be equipped with adaptive headlight systems. This includes dynamic bending light, static cornering light, automatic leveling, and the high beam assist [30]. Systems such as high beam assist and camera-based bending light depend on the front camera to detect surroundings and traffic. They increase illumination and improve driver vision [31], [32]. Since drivers obtain over 90% of information visually, illumination at night is crucial [33]. During the night, crash rates are higher and more severe [34]. Headlights are among the most common PTI defects [35], [36], making checks of cameras and related lighting even more relevant [25].

The high beam assist, as an ADAS, automatically switches high beam on and off depending on [31]:

- Vehicle speed v
- Ambient light
- Other traffic participants nearby

To activate the high beam assist, a vehicle speed threshold of about $v > 60\,\text{km/h}$ (vehicle-dependent) must be exceeded. With the high beam assist enabled, the high beam turns on only if the ambient light is below a threshold and no traffic participants are detected nearby. If ambient light exceeds the threshold or others are detected, the high beam is deactivated or remains off. If the vehicle speed drops below about $v < 20\,\text{km/h}$ (vehicle-dependent), the high beam assist and the high beam are deactivated [25]. The high beam assist disables the entire high beam, depending on the conditions mentioned, and switches to the low beam.

A further development is the *adaptive high beam*, also called *dynamic light assist* [37], *glare-free high beam*, or *Matrix LED Headlight* [38]. The high beam assist then controls the high beam in segments. The front camera detects participants and objects. The control unit evaluates data in real time and disables individual segments. This prevents glare while keeping other segments illuminated. An example is illustrated in Fig. 3.

The red vehicle (a) has an active high beam assist, which controls the adaptive high beam. The red vehicles' (a) front camera detects oncoming (b) and preceding vehicles (c). The system disables the high beam segments at those positions. The remaining areas stay illuminated.

The transition between illuminated and shadowed light segments is the *cutoff line*. Every headlamp must have such a cutoff line in low beam to prevent glare. In a PTI, the horizontal cutoff line of the low beam is checked with a beamsetter. Fig. 4 shows a low beam pattern and the horizontal cutoff line.

The cutoff line has three parts. In (a), the cutoff line is horizontal and defines height. In (b), it rises to illuminate the roadside. In (c), it becomes horizontal again to achieve uniform lateral distribution. Area (d) highlights the vertical transition from shadowed (top) to illuminated (bottom) for the horizontal cutoff line in detail.

With the high beam on, the horizontal cutoff disappears because the high beam emits above. This can glare at oncoming and preceding traffic. With adaptive high beam, new cutoff lines appear. They are no longer horizontal like with a low beam, but vertical. Each shadowed segment yields left and right vertical cutoff lines. Their brightness transition from shadowed to illuminated runs horizontally, i.e., rotated 90° compared to Fig. 4(d).

B. KÜS DRIVE

The KÜS DRIVE (**D**ynamic **R**oadworthiness **I**nspection for **VE**hicles) [41] test lane is a holistic approach to research PTI testability of series vehicles. The legal PTI requirements by StVZO [14] for non-destructive testing without removing parts are met. Detailed descriptions were published by Tentrup et al. [42], [43]. The components relevant to this work are briefly explained.

The main components of KÜS DRIVE are shown in Fig. 5.

The Steerable Function Tester (SFT) (a) holds each wheel on double rollers. The two front roller pairs can steer, so the Vehicle Under Test (VUT) can steer during tests. Without steer, speeds up to 130 km/h are possible. The maximum *allowed* steering angle is approximately 10° and, as indicated

FIGURE 5. Overview of the KÜS DRIVE test lane: (a) Steerable Function Tester, (b) Control station, (c) Radar environment simulation via a radar target simulator, (d) Two laser projectors (right one hidden by the side screen), (e) Environment simulation for the front camera via a screen, (f) Portal system, (g) Projection wall (here in idle position) [41].

by the test bench, decreases with increasing vehicle speed. Typical passenger car wheelbases are adjustable. At the control station (b), the test bench is configured, and test runs are started. A screen (e) simulates the environment for the front camera, and a radar target simulator (c) stimulates the radar. Both are mounted on the portal (f) and positioned automatically in front of the respective sensor. The screen (e) outputs an Aurelion simulation [44] by dSPACE [45] to stimulate the camera. Objects in the simulation can also be output by the radar target simulator (c) to stimulate the VUT radar. The rear projection wall (g) serves as a defined surface for the laser projectors (d). The projection wall (g) can be in idle position as in Fig. 5 or lowered in working position as in Fig. 6. The two laser projectors (d) are installed on the left and right front of the projection wall.

Fig. 6 shows the KÜS DRIVE during a test run.

In a test run, the VUT (d) accelerates on the SFT to a defined speed. Depending on the test scope, different checks are automated. In the example shown in Fig. 6, the screen (b) stimulates the front camera with a dynamic simulation. The VUT is represented as a point of view (POV) within the simulation, with its movements being continuously mirrored and executed in real time. The radar target simulator (c) is positioned in front of the radar sensor and emits signals representing the target. In parallel, the laser projectors draw the current position and dimensions of the target vehicle as a green contour on the projection wall (a), based on the relative distance between the target vehicle and the VUTs POV. This contour is a bounding box that corresponds to a vehicle outline in this setup, although a classical rectangular shape is also possible. On the projection wall, the laser projections

FIGURE 6. KÜS DRIVE during a test run [41]: (a) Laser projection of the target vehicle on the projection wall lowered in working position, (b) Screen extended in front of the VUT for front camera stimulation. The simulated target vehicle is visible as a preceding car, (c) The radar target simulator with absorbers (only partly visible from this angle). The stimulator is extended exactly in front of the VUT radar, (d) VUT.

overlap with the real headlight pattern of the VUT. Through visual inspection, it can then be verified whether the adaptive high beam segments are correctly shadowed and properly aligned with the projected target position.

A central compute and control unit synchronizes all subsystems so that simulation, sensor stimulation, and laser projection align in time and dimension. The target vehicle in the simulation is output on the screen for the camera, via the radar target simulator for radar, and as a laser projection on the projection wall in sync.

KÜS DRIVE can thus examine adaptive headlight systems for glare-free operation and illumination. In this context, a patent application has also been filed describing a test bench-based verification of adaptive headlamp beam patterns using a projection wall and camera-field stimuli

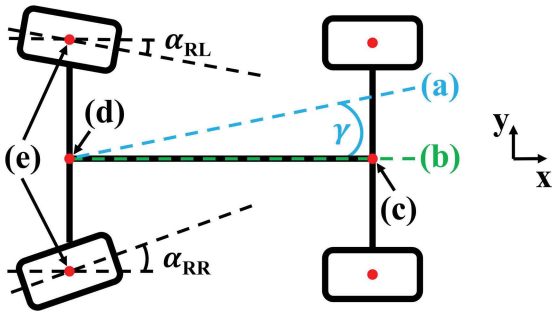

FIGURE 7. Example axle geometry in top view: (a) Direction of the thrust axis, (b) Vehicle symmetry axis, (c) Front axle midpoint, (d) Rear axle midpoint, (e) Wheel centers rear left and rear right, (γ) Thrust angle between direction of the thrust axis and vehicle symmetry axis, (α_{RR}) Toe angle rear right, (α_{RL}) Toe angle rear left. After [47].

(DE 10 2022 102 328 A1) [46]. Furthermore, ADAS such as intelligent speed assistance, autonomous emergency braking system, Adaptive Cruise Control (ACC), and lane keeping assist/lane departure warning system can be dynamically stimulated and checked for functional safety. Anti-lock braking system, electronic stability program, and traction control system can be tested in defined scenarios under controlled conditions. The integrated environment enables complex, reproducible, and automated test scenarios across the vehicle life cycle [41].

C. VEHICLE GEOMETRY AND SENSOR ALIGNMENT

Understanding this work requires a basic knowledge of vehicle axle geometry, which is explained below. Fig. 7 shows an example of an abstract vehicle in top view.

The abstract vehicle with four wheels travels along the x-axis. The wheel centers of the two front wheels define the midpoint of the front axle (c), while the wheel centers of the two rear wheels (e) define the midpoint of the rear axle (d). The line connecting both axle midpoints (c) and (d) defines the vehicle's *symmetry axis* (b), which is parallel to the x-axis in this example. The planes of the front wheels are parallel to the x-axis in this example, resulting in a front wheel toe angle of 0°. The rear wheels, however, have inward toe angles α_{RR} and α_{RL}.

The *geometric thrust axis* represents the actual direction in which the vehicle moves, depending on the rear wheel toe angles. The geometric thrust axis deviates from the vehicle's symmetry axis by the *thrust angle* γ, also called yaw angle, which can be calculated as [47]

$$\gamma = \frac{\alpha_{RR} - \alpha_{RL}}{2}. \tag{1}$$

This highlights a key distinction: the vehicle's symmetry axis deviates from the thrust axis by the thrust angle. The headlights are aligned with the symmetry axis [48], whereas environmental sensors such as the front camera are aligned with the thrust axis [49], [50]. As a result, a systematic offset occurs between road illumination and object detection, which is typically compensated by calibration.

III. METHODS AND EXPERIMENTAL

A. METHOD DERIVATION AND ADAS SELECTION

The proposed workflow follows an *input–process–output* principle. In particular, PTI stakeholders and other independent third parties do not have access to proprietary in-vehicle data, internal control logic, or OEM-specific implementation details. Consequently, the vehicle must be treated as a *closed box*. Under this constraint, it becomes essential to select an output signal that is (i) observable from outside, (ii) reproducibly triggerable, and (iii) sufficiently informative to draw conclusions about the vehicle's overall perception-and-decision chain. ADAS provide such an output: they can be activated based on defined requirements and can be stimulated by controlled scenarios, while the expected system response is defined by the ADAS itself.

In general, different ADAS depend on different sensing modalities, either through a dominant sensor technology or through sensor fusion. For instance, systems such as ACC are commonly radar-dominated, whereas other systems may rely more strongly on camera perception. However, this dependency cannot be generalized without OEM knowledge, as some manufacturers implement different sensor configurations and fusion strategies (e.g., camera-only approaches [51]) that alter which sensor contributes most to a given ADAS response.

The primary objective of this work is the assessment of the front camera as an environmental sensor. Several ADAS could, in principle, be used to observe a vehicle response that depends on camera perception, including lane keeping assistance, lane change assistance, Automatic Emergency Braking (AEB), and high beam assistance. Nevertheless, these candidate outputs differ significantly in their suitability for the intended verification task. Lane keeping and lane change assistants predominantly exploit information in the lower region of the camera image, as lane markings and near-field road geometry are typically detected there. This would limit the method's coverage of the camera's Field of View (FOV) and thus restrict the interpretability of negative results to a comparatively narrow image region.

AEB responses are likewise constrained in practice. While the relative position of a target object could be varied, an AEB intervention is only expected when a collision becomes imminent. Hence, meaningful stimulation typically requires the target to remain in front of the vehicle, again limiting usable FOV coverage. In addition, AEB-based testing is not robustly realizable with real target carriers at the available test bench, such that the evaluation would be largely confined to simulation-only trials.

For these reasons, (adaptive) high beam assistance was selected as the most suitable observable output for the proposed closed-box verification approach. First, other road users can be positioned both in real and simulated scenarios across a wide range of angular positions, enabling stimulation over a substantially larger portion of the front camera's FOV. Second, the system response is directly perceivable: in particular, the selective shading of individual high-beam segments

provides an immediate and intuitive indication of the perceived object position and the resulting decision of the ADAS. This yields a practical advantage for PTI-oriented workflows, as the response can be assessed visually by an inspector without requiring access to proprietary in-vehicle signals.

It is important to emphasize that the proposed method does not aim to diagnose the root cause of a detected malfunction (e.g., pixel defects) in the context of PTI. Instead, the approach is designed to reveal whether the camera-dependent system exhibits plausible operational behavior under controlled stimulation. For example, degradations caused by obscuration, contamination, or windshield damage—which are already subject to visual inspection in current PTI procedures as part of the PTI test criteria *condition*—may manifest as incorrect shading patterns or missing reactions. From a PTI perspective, however, determining the precise technical cause is not required: the inspection's core task is to assess whether the system shows correct operational performance. If not, detailed diagnosis and repair are typically performed subsequently in a workshop environment rather than within the PTI itself.

B. TEST OVERVIEW AND SETUP

Three tests were conducted to investigate a front camera verification method at the Vehicle-in-the-Loop test bench KÜS DRIVE under PTI constraints. All tests follow the *Input-Process-Output* principle shown in Fig. 1 [24], with a slight modification. Instead of simulated stimuli, real physical objects were used for camera stimulation. This enabled a targeted stimulation of the front camera (*Input*), closed-box internal processing by the vehicle's perception system (*Process*), and an evaluation of the vehicle reaction via the high beam assist using adaptive high beam (*Output*). In contrast to previous low-cost approaches that relied on full high beam deactivation [24], [25], the adaptive high beam is now utilized to shadow individual segments selectively. All tests were carried out on KÜS DRIVE. During testing, the VUT drove on the SFT with adaptive cruise control activated at approximately 70 km/h. The resulting headlight pattern was projected onto the projection wall and recorded on video, allowing detailed analysis of the vertical cutoff lines between illuminated and shadowed segments. This video-based approach was selected because, if it proves robust in practice, it would easily enable an automated and time-efficient evaluation that is realistically implementable within PTI workflows, where short test durations and practicable instrumentation are critical. Table 1 provides an overview of the three test configurations.

Test I. Static LED lights act as the stimulus. The objective is to demonstrate that the ViL test bench can reliably trigger a vehicle reaction by shadowing individual light segments, thereby establishing a proof of concept for a *function* check of the front camera. The evaluation examines whether the correct adaptive high beam segments are shadowed and measures the distance between the LED light center and the vertical cutoff line. In addition, the influence of deliberately simulated modifications of the vehicle's axle geometry during front camera calibration on the position of the headlight cutoff line is analyzed. Further details are provided in Section III-C.

TABLE 1. Overview of the tests conducted in this work.

Test	Target	Stimulation	Output
I	Proof of concept for *function* check, Influence of camera calibration & axle geometry	Static LED lights	Distance: LED light center ↔ vertical headlight cutoff line (left/right)
II	*Efficiency* check, VUT comparison	Dynamic LED lights	Distance profile: LED light center ↔ vertical headlight cutoff line (left/right)
III	*Efficiency* check, VUT comparison, Simulation	Dynamic simulated target vehicle	Distance profile: Target vehicle bounding box ↔ vertical headlight cutoff line (left/right)

Test II. LED lights are moved horizontally in front of the VUT. The objective is to verify the consistency of vehicle reactions to realize an *efficiency* check. The evaluation analyzes the distance profile between the center of the moving LED light and the vertical cutoff line. Furthermore, differences between VUT (Škoda Octavia, Volkswagen Passat, Ford Focus) are investigated, see Section III-D.

Test III. A dynamic simulated target vehicle is generated with Aurelion software [44] and displayed on a screen in front of the front camera as the stimulus. The objective is to verify the consistency of reactions in a highly reproducible simulated environment. The evaluation determines the distance profile between the bounding box edges and the vertical cutoff lines. In addition, differences between the VUT (Škoda Octavia, Volkswagen Passat, Ford Focus) are investigated, see Section III-E.

1) TEST ENVIRONMENT

All tests were conducted at KÜS Bundesgeschäftsstelle on the KÜS DRIVE test lane [41]. The test chamber was darkened to prevent ambient light from entering.

2) TEST VEHICLES

Three vehicles were used:

- Škoda Octavia (Station Wagon, 2022)
- Volkswagen Passat (Station Wagon, 2024)
- Ford Focus (Station Wagon, 2019)

Each vehicle features an adaptive headlight system and a high beam assist. The same driver performed all tests. No other persons were in the vehicles. The VUTs were not additionally loaded (only the usual equipment in the spare wheel well was used).

3) TEST EQUIPMENT

The following test equipment was used for the tests:

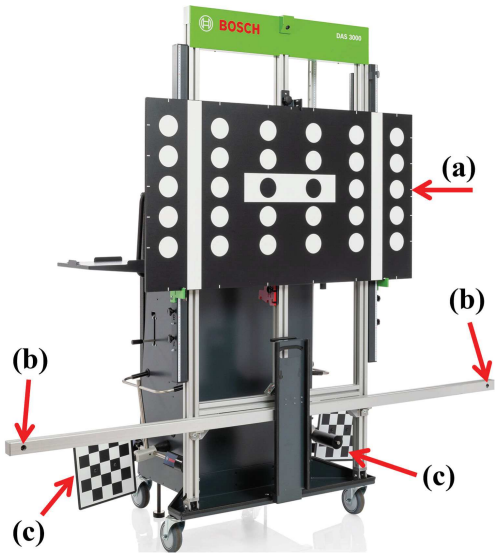

FIGURE 8. Mobile calibration system BOSCH DAS3000 S20 [52] with (a) calibration target 1681098011 (CTA 300-1), (b) two cameras in the camera bar, (c) reference targets (CTA 400-1) with wheel holders (CTA 100-1), shown here just stored on the DAS3000 [55].

- Calibration system BOSCH DAS3000 S20 [52]
- Camera GoPro HERO11 Black [53]
- LED lights (Model: ZQ01430) [54]

The BOSCH DAS3000 S20 [52], shown in Fig. 8, is a mobile calibration system for ADAS.

The DAS3000 was used to calibrate the front camera of the VUT. The DAS3000 consists of a calibration target (CTA 300-1) (a), two cameras in the camera bar (b) for correct positioning of the calibration system relative to the VUT, and two reference targets (CTA 400-1) with wheel holders (CTA 100-1) (c) that are attached to the VUT. The calibration process consists of several consecutive steps, which are described in the manual [55]. The process is briefly summarized below:

1) **Mounting the reference targets:** First, the two reference targets (CTA 400-1) are mounted on the rear right and front left wheels. The wheel holders (CTA 100-1) are fixed directly to the tire via four contact points (see Fig. 9(b)). The spirit level on each reference target is adjusted until the plates are precisely leveled (see Fig. 9(c) and (d)).
2) **Connecting the vehicle diagnostics:** The additional diagnostic module KTS 560 is connected to the VUT via the OBD interface. Using the ESI[tronic] software (Version 2025/1.1.07.002), the system automatically identifies the vehicle data and prepares the calibration procedure. The software then guides step by step through the calibration.
3) **Capturing the reference targets:** The DAS3000 uses two integrated cameras in the camera bar to capture the reference targets and determine their spatial position.
4) **Repositioning the reference target:** After capture, the front left reference target is removed from the wheel and reattached to the rear left wheel (see Fig. 9(a)). The reference targets are now positioned at the rear left and rear right wheels.
5) **Positioning the DAS3000:** The chassis of the DAS3000 is moved in front of the vehicle into its working position. The ESI[tronic] software indicates the correct position and is reached by sliding the chassis. The parking brake on the chassis is then engaged to secure the system.
6) **Height measurement at the vehicle:** The vertical distances between the lower edge of the fender and the tire contact patch are measured for each wheel and entered into the software. These values are used to precisely reference the vehicle geometry within the calibration system.
7) **Completion of the calibration:** Finally, the ignition of the VUT is switched off and restarted after a few seconds. The software confirms successful calibration and outputs the angle values of the front camera: yaw angle, pitch angle, and roll angle.

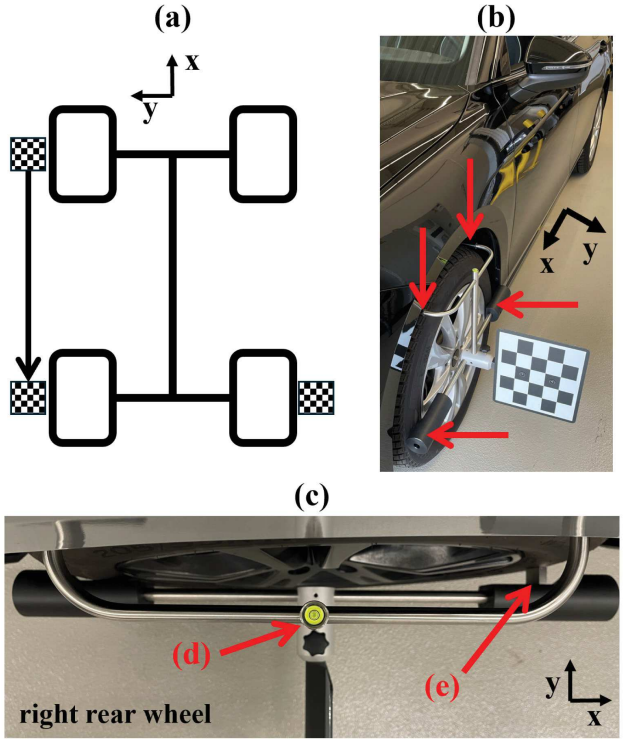

FIGURE 9. Details during the calibration of the front camera with the DAS3000: (a) Positioning of the reference targets on the vehicle under test. First at the front left and rear right, then at the rear left and rear right. (b) Example of the reference target mounted on the front left wheel, red marks indicate the four contact points between tire and wheel holder, (c) Example at the right rear wheel from an almost vertical top view with the leveled spirit level visible (d) and a gauge block (e) attached from the wheel center in positive x-direction, which is used and explained in III-C.

Fig. 9 shows details of the calibration process.

The reference targets are initially attached to the front left and rear right wheels of the VUT. During the process, the front left reference target is moved to the rear left. The rear

right reference target remains mounted for the entire calibration process (a). The wheel holder is fixed via four contact points on the tire (b). Two contact points lie on the wheel tread, and two on the wheel sidewall. The reference target is adjusted until the spirit level (d) is precisely leveled. In (e), a gauge block is shown that was inserted at the contact point to change the distance and alignment of the wheel holder. This gauge block is later used in Section III-C to simulate a deliberate change in toe angle at the right rear wheel only. Standard calibration procedures are performed without the use of a gauge block.

For video recording of the projection wall, a GoPro HERO11 Black [53] (Firmware v02.32.00) was used. The GoPro was set to 4K, 60 fps, linear perspective, and 2× zoom and was firmly installed at the portal system of KÜS DRIVE. The GoPro was aligned with the projection wall, onto which the headlight pattern of the VUT was projected, and recorded this pattern during all tests. An external power supply (power bank) ensured that no cable connection was required after installation. Operation via the touch display was unnecessary due to remote control via app, so the camera remained untouched throughout all tests and retained constant alignment and position.

As vehicle taillights, the LED stage lights ZQ01430 were used [54]. The LED lights were always operated in red color at maximum brightness, selected via the remote control presets.

C. TEST I: REAL LED LIGHTS - STATIC

The objective was to verify the basic method of Fig. 1 (proof of concept) and to determine the influence of the thrust angle γ on the VUT high beam pattern. Different rear right wheel toe angles were simulated across several front camera calibrations. Two LED lights served as the stimulus, imitating the taillights of a preceding vehicle. For each calibration state, the distance between the headlight cutoff line and the center of each LED light was evaluated.

1) EXPERIMENTAL SETUP

The LED lights were positioned on a trolley at a height of 0.92 m with a horizontal spacing of 0.80 m. This positioning, used to emulate the rear lamps of a vehicle, complies with the installation requirements specified in UNECE Regulation No. 48 [56]. In particular, Regulation No. 48 does not prescribe a minimum distance between the inner edges of the apparent luminous surfaces for vehicle classes M1 and N1, whereas for other vehicle classes a minimum of 0.60 m is required. The setup in this work meets this requirement with a spacing of 0.80 m. Regarding height, rear lamps are generally required to be mounted between 0.35 m and 1.50 m above the ground, which is satisfied by the selected trolley height of 0.92 m. To avoid reflections of the VUT, both LED lights were rotated inward by approximately 10°. The trolley was covered with dark matte fleece to minimize residual reflections and was placed centrally and as close as possible to the projection wall.

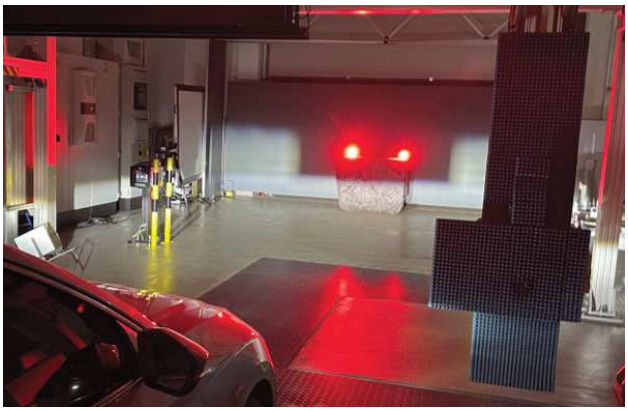

FIGURE 10. Setup for Test I: LED lights — static. Bottom left: front of the VUT (Škoda Octavia). On the projection wall, the trolley with active LED lights and the shadowed AFS segment are visible. Right edge: radar target simulator, top left: screen. Neither was used here and was in an idle position outside the VUT field of view.

The Škoda Octavia front camera was calibrated with the BOSCH DAS3000. To vary the apparent toe of the rear right wheel, defined gauge blocks were inserted between the wheel holder with reference target and the tire (Fig. 9(e)). During a normal calibration, the wheel holder with the reference target at the rear right remains mounted in the same position. With an inserted gauge block, the alignment of the wheel holder and thus the reference target changes. The DAS3000 detects the simulated change in alignment and updates the front camera correction parameters of the VUT during calibration, without any mechanical adjustment.

Gauge blocks were used at two positions: in driving direction x from the wheel center, which makes the toe of the rear right wheel apparently more negative (Fig. 9(e)), and opposite to the driving direction x, which makes the toe apparently more positive. In total, five calibrations were performed:

- 3 cm gauge block in driving direction x
- 2 cm gauge block in driving direction x (see Fig. 9)
- Normal calibration without gauge block
- 2 cm gauge block opposite to driving direction x
- 3 cm gauge block opposite to driving direction x

2) IMPLEMENTATION

After each calibration, the VUT accelerated on the SFT to approximately 70 km/h to provide a safety margin above the 60 km/h threshold for activating the high beam assist. The driver then activated ACC at 70 km/h to keep the speed constant. Steering inputs were minimized to keep the lateral position on the SFT steady. As soon as the high beam assist enabled the adaptive high beam, the test run continued.

The LED lights were initially off and were switched on and off five times per calibration using the remote control. Approximately 3 s were waited between switching events to allow a vehicle reaction. The GoPro HERO11 Black recorded the projection wall with the resulting headlight pattern continuously. Fig. 10 shows the setup during the test execution.

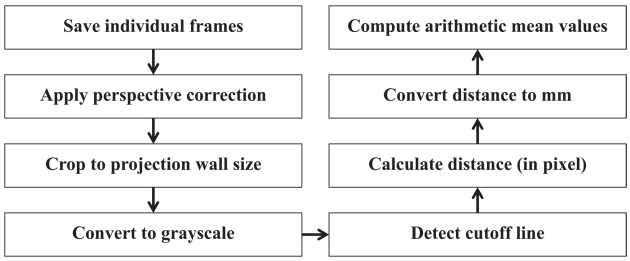

FIGURE 11. Evaluation process for Test I with static LED lights.

In Fig. 10, the VUT is on the SFT with ACC in constant-speed mode. The trolley, covered with matte fleece, stands in front of the projection wall, with the LED lights mounted on it. The LED lights are active and shine red. The projection wall shows the high beam pattern of the VUT. The adaptive high beam shadows the segment at the position of the red LED lights. The radar target simulator with absorber mats is visible at the right edge of the image. The lower edge of the environment simulation screen is visible at the upper left edge of the image. The radar target simulator and the screen were not used in this test and remained in an idle position outside the VUT field of view.

3) EVALUATION

One video was recorded per calibration. Each video captures the vehicle's response to five consecutive LED activations. To enable a consistent and reproducible analysis, an evaluation workflow was defined before conducting the experiments. The workflow structures the video-based assessment into eight successive steps. The individual steps are summarized in Fig. 11 and described in the following.

a: SAVE INDIVIDUAL FRAMES

In each video, the vehicle reacted five times to the activating LED lights. The GoPro recorded at 60 fps. A high frame rate should be targeted to capture changes in the light pattern with high temporal resolution, enabling rapid and reliable detection of reaction onsets across consecutive frames. The reaction spanned multiple frames until the headlight pattern and the shadowed segment stabilized, with the stable state persisting over the approximately 3 s waiting duration. As the trolley remained static, the pattern and the shadowed segment remained constant. Exact frame selection was therefore uncritical. The decisive point was that the chosen frame lay *after* the vehicle reaction and stabilization of the pattern and *before* the next LED off event. Frames between these points were equivalent for evaluation. Starting at the reaction onset, the video was inspected frame by frame. The first frame with a stable pattern was extracted. Across the five videos, 25 frames were extracted.

b: APPLY PERSPECTIVE CORRECTION

The GoPro mounted on the portal system had a slightly top-down view. A perspective rectification was performed to obtain absolute distances. The basis was a projective mapping (homography) to a right-angled target rectangle. The target rectangle was the projection wall. Pixel coordinates of the four wall corners were manually measured in one original image using Microsoft Paint (Version 11.2504.551.0). Since the pose and position of the GoPro did not change, coordinates from a single image were sufficient. The mapping in homogeneous coordinates was

$$\lambda \mathbf{q} = \mathbf{H}\mathbf{p}, \qquad \mathbf{H} \in \mathbb{R}^{3\times 3},\ \lambda \neq 0 \tag{2}$$

with homogeneous source point $\mathbf{p} = (x, y, 1)^\top$, homogeneous target point $\mathbf{q} = (u, v, 1)^\top$, and scale λ. The homography $\mathbf{H}$ was computed from four correspondences and then applied to the image using bilinear interpolation. The implementation used Python with OpenCV (`cv2.getPerspectiveTransform` for $\mathbf{H}$ and `cv2.warpPerspective` for warping).

c: CROP TO PROJECTION WALL SIZE

After rectification, the new pixel coordinates of the four wall corners were read using Microsoft Paint. The quadrilateral defined a fixed axis-aligned crop of the projection wall. The same crop was applied to all 25 images to extract only the relevant content from the projection wall.

d: CONVERT TO GRAYSCALE

The color images were converted to 8-bit grayscale using OpenCV (`cv2.cvtColor`). Each pixel has a brightness value in $[0, 255]$, where zero is black and 255 is white. Grayscale emphasizes the headlight cutoff line, facilitating its detection.

e: DETECT CUTOFF LINE

This step establishes the key supporting method of this work: a practical definition to determine the cutoff line, which is not described in this form in the existing literature. The objective is to propose a first, implementable approach for cutoff line detection and to validate its applicability within the conducted experiments. The procedure was designed to be as robust and reproducible as possible, which is essential for a potential use in the PTI context. Fig. 12 illustrates the procedure and facilitates its understanding.

Fig. 12 shows a GoPro frame of the projection wall (a) and the result after processing (b). The complete projection wall, the LED lights on the trolley with centers P_L and P_R, the areas illuminated by the adaptive high beam (c), and the shadowed segment (d) are visible.

Due to a lack of established methods in the literature, a proprietary procedure was developed iteratively to determine the headlight cutoff lines C_L and C_R. Perception of a cutoff line can be subjective at high magnification. Typically, a bright region, a transition, and a dark region (or vice versa) exist, as described in Fig. 4(d). The objective was not absolute, subpixel accurate positioning. The objective was to develop a method that defines cutoff lines consistently across images, enabling objective comparison.

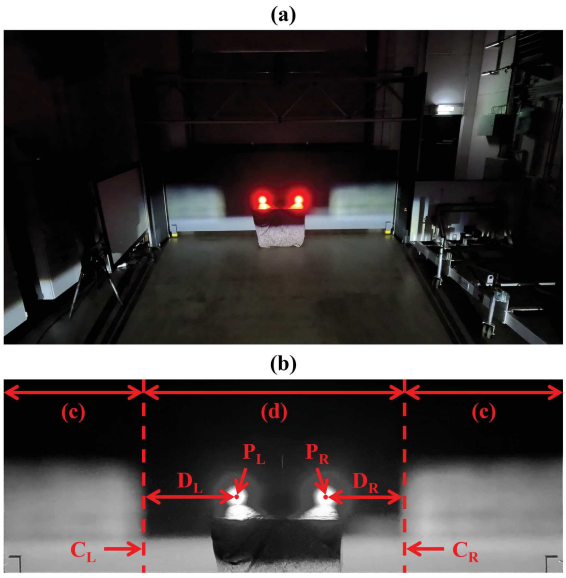

FIGURE 12. Example frame in the original state (a) and after the preceding processing steps (b). Visible are the areas illuminated by the adaptive high beam (c) and the shadowed segment (d). The LED light centers are at P_L and P_R.

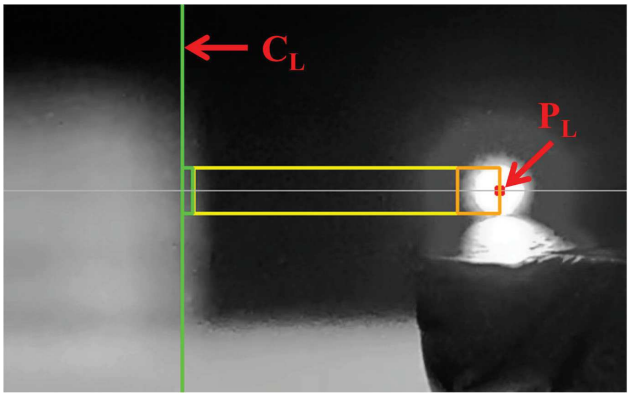

FIGURE 13. Detail for determining the headlight cutoff line (C_L for the left LED center P_L).

The procedure is illustrated in Fig. 13. Only the left image section is shown to highlight relevant pixels with auxiliary guides and to explain the determination of the cutoff line.

The starting points are the LED light centers $P_L = (x_L, y_L)$ and $P_R = (x_R, y_R)$. For Test I, the light centers were determined manually in Microsoft Paint once and used consistently for all images. Only P_L is shown in Fig. 13. The basic principle is as follows: from the left LED light center, pixels are scanned successively to the left starting at $x_L - 1$. From the right LED light center, pixels are scanned to the right starting at $x_R + 1$. For each tested column x, the brightness $B_{single}(x)$ is evaluated at row y_0 with $y_0 = y_L$ or y_R. In Fig. 13, this common row is the light gray horizontal line. If at least s consecutive columns exceed the threshold T, i.e., $B_{single}(x) > T$, the cutoff line is defined at the *last* column of that series. This yields C_L for the left search and C_R for the right search. In Fig. 13, the s consecutive columns are framed in light green next to the vertical light green cutoff line.

Robustness was increased in two steps. First, instead of using single-pixel values, a vertical mean was calculated over a window of ± 20 pixels around y_0. In Fig. 13, this window corresponds to the height of the colored frames. The column-wise mean brightness is

$$B_{mean}(x) = \frac{1}{41} \sum_{y=y_0-20}^{y_0+20} B_{single}(x, y). \tag{3}$$

This averaging reduces noise, local outliers, and inhomogeneous illumination.

Second, before a series with $B_{mean}(x) > T$ begins, at least one column with $B_{mean}(x) < T$ is required. This explicitly captures the transition from a region of lower brightness to a region of higher brightness, thereby avoiding false detections along bright headlight outlines. From there, s consecutive columns with $B_{mean}(x) > T$ are sought.

In Fig. 13, this is visible as follows: pixels within the orange-framed window still lie in the bright headlight region. Only at the transition to the yellow-framed window does $B_{mean}(x) < T$ first become true, and the search for s consecutive columns with mean brightness above T begins. The yellow and green windows define the search zone. In the yellow window, some column means repeatedly falling below T. In the green window, s consecutive columns satisfy $B_{mean}(x) > T$, which determines the headlight cutoff line in the last of the s consecutive columns.

The parameters s and T were determined iteratively in pretests (resulting in $s = 10$ and $T = 80$) and were then applied consistently for all evaluations. To derive T, several grayscale images were first inspected manually and the vertical position (y) of the LED centers was determined (e.g., using a simple image viewer). At this height, the horizontal pixel intensity profile was extracted and the luminance values around the cutoff line transition were analyzed. It was observed that the dimmed dark segments typically showed values up to approximately 30, whereas the illuminated bright side exhibited values from about 130 upward, with a transition band in between. The threshold was therefore set to $T = 80$ as a mid-point between the identified bounds to locate the cutoff line approximately in the middle of the dark-to-bright transition.

Similarly, the parameter s was introduced to improve robustness, because isolated outliers occurred when relying on single-column intensity changes. By requiring a transition to persist over s consecutive columns, local interferences and sporadic artifacts are suppressed and the detection becomes more stable. Thus, neither along the vertical extent (y) nor along the horizontal direction (x) is the evaluation based on a single pixel value; instead, it leverages small local neighborhoods, which is more robust against outliers and minor inconsistencies in the projected vehicle light pattern.

The exact numerical values are less critical as long as they are not chosen substantially lower or higher; for instance, $T = 75$ or $T = 85$ and $s = 8$ or $s = 12$ would likely lead to similarly reproducible results. The key requirement for this

work is that the parameters are fixed and applied consistently to ensure comparability across all runs. As this study is the first to introduce a reproducible computational procedure for cutoff line detection within the presented workflow, this level of justification is sufficient to enable discussion of the results. For a future PTI application, the parameters should be analyzed in more detail and then standardized to ensure comparability across PTI institutions.

f: CALCULATE DISTANCE (IN PIXEL)

Distances between LED light centers and cutoff lines were defined by differences of x-coordinates (see Fig. 12). The LED light centers are $P_L = (x_L, y_L)$ and $P_R = (x_R, y_R)$. The cutoff lines are vertical lines C_L and C_R at x_{CL} and x_{CR}. The horizontal distances are

$$D_L = |x_L - x_{CL}| \qquad D_R = |x_R - x_{CR}|. \tag{4}$$

In all 25 images, P_L, P_R, C_L, and C_R were overlaid to enable visual plausibility checks. Given the limited number of images, this manual control step was feasible.

g: CONVERT DISTANCE TO mm

A linear scaling factor z was determined to convert pixel coordinates to metric distances. The basis was the known physical dimensions of the projection wall and the corresponding pixel dimensions of the cropped image, which equals the projection wall. For the horizontal direction

$$z_{\text{horizontal}} = \frac{W_{\text{phys}}}{W_{\text{px}}} \quad [\text{mm/px}], \tag{5}$$

with physical wall width W_{phys} and pixel width W_{px}. Analogously for the vertical direction

$$z_{\text{vertical}} = \frac{H_{\text{phys}}}{H_{\text{px}}} \quad [\text{mm/px}], \tag{6}$$

with wall height H_{phys} and pixel height H_{px}. The analysis used $z_{\text{horizontal}}$ exclusively, since only lateral distances of cutoff lines are relevant. z_{vertical} was used to verify rectification and to estimate residual distortions.

h: COMPUTE ARITHMETIC MEAN VALUES

For each calibration state, D_L and D_R from the five LED activations were averaged arithmetically. This yields a robust representation per calibration state and reduces random variation.

With this procedure, Test I was evaluated. Results are presented in Section IV-A.

D. TEST II: REAL LED LIGHTS - DYNAMIC

The objective was to analyze the distance between the headlight cutoff line and the center of the dynamically moved LED lights. In contrast to Test I, no thrust angle change was simulated. Instead, the LED lights on the trolley were moved dynamically. Three VUTs were used: Škoda Octavia, Volkswagen Passat, and Ford Focus.

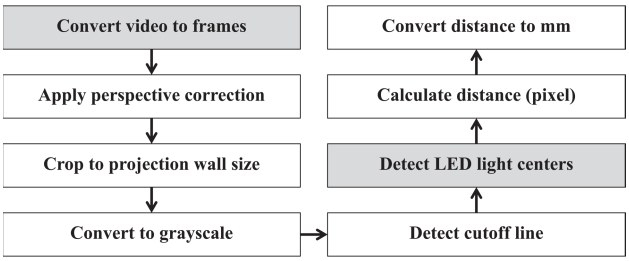

FIGURE 14. Evaluation process for the Test II with dynamic LED lights. Gray shading marks new or adapted steps compared to Test I in Fig. 11.

1) EXPERIMENTAL SETUP

The trolley with the LED lights was moved horizontally in front of the projection wall. Thus, Test II extends the static target of Test I to a dynamic target. A floor guide ensured motion was as straight, close to, and parallel to the projection wall as possible. The trolley wheels glided along the floor guide. The trolley was pulled linearly and did not yaw laterally. Hence, the distance between the trolley and the projection wall, as well as between the VUT and the LED lights, remained constant. Lashing straps were attached to the trolley, allowing personnel to move it from outside the headlight and projection area.

The motion followed a fixed sequence: start at the right edge of the projection wall, translate the trolley at approximately constant speed of $0.11\,\text{m}\,\text{s}^{-1}$ to the left edge, then return to the starting position. The speed was kept as constant as possible. Some variation remained due to manual operation.

The GoPro HERO11 Black recorded the projection wall continuously. In this way, the reactions of the adaptive high beam to the dynamically moving LED lights were documented, generating a distance profile.

2) IMPLEMENTATION

Each vehicle was prepared as in Test I (see Section III-C.2). After activation of the high beam, the VUT was on the SFT with ACC at a constant speed. The LED lights on the trolley, in their start position, were then switched on, causing them to shine red. The described motion sequence started. The projection wall with the headlight patterns was recorded throughout. The test ended once the trolley returned to its starting position at the right edge of the projection wall.

3) EVALUATION

Video evaluation followed the general process of Test I (see Fig. 11 in Section III-C.3). The process required adaptations. Fig. 14 shows the adapted process.

The step *Save individual frame* was replaced by *Convert video to frames*. The step *Detect LED light centers* was added. The step *Compute arithmetic mean values* was omitted compared to Test I (see Fig. 11 in Section III-C.3). The adapted and added steps are highlighted in gray in Fig. 14. The following explains only these steps.

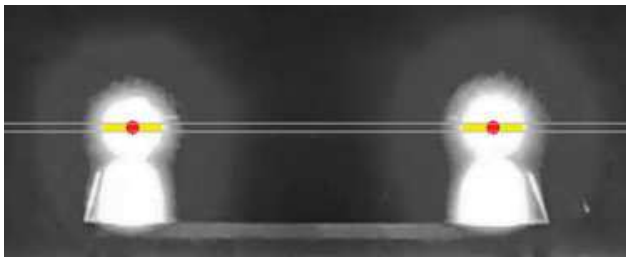

FIGURE 15. Example of detecting LED light centers. Yellow: candidate LED regions. Red: intensity centroid for each region.

a: CONVERT VIDEO TO FRAMES

One video was recorded per VUT. Each video was first trimmed to start at LED activation and end at the moment the trolley returned to its original position. The trimmed video was then exported as individual frames, yielding a substantially larger number of images. Automated processing was therefore mandatory. Such automation is not only practical for the experimental evaluation, but also highly relevant for potential PTI deployment: given the proposed workflow, an automatic analysis can be implemented with comparatively low effort and could be integrated into a routine inspection process. For instance, the stimulation could be performed at the beginning of the PTI sequence, while the evaluation runs in parallel, such that the results are available by the end of the inspection. Alternatively, the relevant distances could be computed in real time and directly displayed after a single test run to indicate whether deviations suggest a deficiency.

b: APPLY PERSPECTIVE CORRECTION

c: CROP TO PROJECTION WALL SIZE

d: CONVERT TO GRAYSCALE

e: DETECT CUTOFF LINE

See Section III-C.3.

f: DETECT LED LIGHT CENTERS

Because the LED lights were moved dynamically, their positions changed from one frame to the next. Their centers could not be assumed static. They had to be re-estimated in every image. Detection followed a fixed sequence: build a brightness profile, identify bright regions, compute intensity-weighted centroids, and finally select a valid pair using the known LED spacing. Fig. 15 provides an overview.

A fixed reference height was determined from an example frame as $y_0 = 344$ px. Because the LED lights moved only horizontally, a small vertical window of ± 3 pixels around y_0 was evaluated to smooth minor vertical fluctuations and local outliers (light gray horizontal lines in Fig. 15). For each column x, the mean grayscale within this band was computed. The horizontal brightness profile $B(x)$ is

$$B_{horizontal}(x) = \frac{1}{7} \sum_{y=y_0-3}^{y_0+3} B_{single}(x, y). \tag{7}$$

All columns with $B_{horizontal}(x) > 240$ were then identified. This threshold was determined iteratively. Adjacent above-threshold columns were grouped into intervals, each representing a candidate LED region (yellow in Fig. 15. An interval is described by its bounds $[r_{\text{start}}, r_{\text{end}}]$.

For each interval, the center was computed as the intensity centroid, using brightness as weight.

$$x_{center} = \frac{\sum_{x=r_{start}}^{r_{end}} x \cdot B(x)}{\sum_{x=r_{start}}^{r_{end}} B(x)} \tag{8}$$

The resulting point representing a region's center was defined as $P = (x_{center}, y_0)$ and is shown in red in Fig. 15.

Finally, all detected centers were validated in pairs. The horizontal distance of the LED light centers had been measured in an example frame as 267 px. A pair was accepted if the horizontal distance matched the known physical LED spacing of 267 px within a tolerance of ± 5 px.

$$|(x_{\text{R}} - x_{\text{L}}) - 267| \leq 5 \tag{9}$$

The first valid pair was taken as the left and right LED lights. This yielded consistent and reproducible centers $(P_{\text{L}}, P_{\text{R}})$ for every frame. For validation, the analyzed frames were skimmed manually. Red points lie plausibly at the LED centers. Exact pixel-perfect alignment was not required. Correct detection could be confirmed in all cases.

g: CALCULATE DISTANCE (PIXEL)

h: CONVERT DISTANCE TO mm

See Section III-C.3.

In contrast to Test I, arithmetic averaging of distances was omitted. The continuous motion of the LED lights yields a series of frames with varying distances, known as the distance profile. This distance profile provides the required information about the adaptive high beam reaction in response to the dynamic LED light position.

Using this process, Test II was evaluated. Results are presented in Section IV-B.

E. TEST III: SIMULATED TARGET VEHICLE - DYNAMIC

The objective of Test III was to transfer the dynamic *efficiency* assessment of Test II into a simulation-based stimulation environment to increase reproducibility. Instead of physical LED lights, a virtual target vehicle was generated in the simulation and displayed on a screen in front of the VUTs front camera. The evaluation concept remained identical to Test II: the lateral distances between the vehicle reaction (vertical headlight cutoff positions on the projection wall) and the target representation were analyzed over time. In Test III, the target was represented by a rendered bounding box, and the distances were computed between the bounding-box edges and the corresponding cutoff positions.

1) EXPERIMENTAL SETUP

The VUT drove on the SFT with ACC active and the high beam assist enabled, as in Test I (Section III-C) and Test II

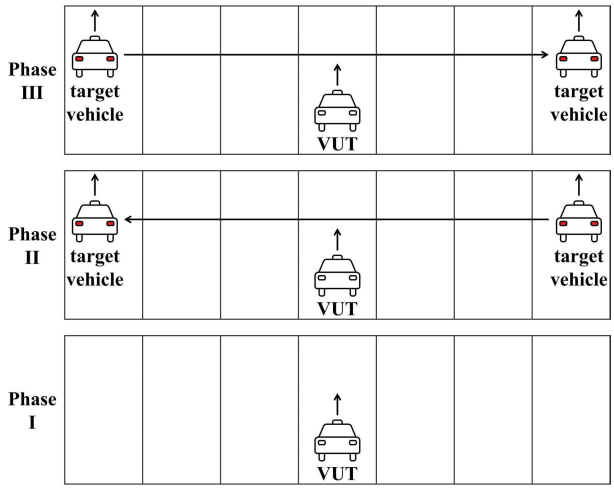

FIGURE 16. Sequence of the environment simulation: Phase I establishes a stable driving situation. Phase II starts the simulation and moves the target vehicle to the center of the left lane. Phase III returns the target vehicle to the right starting position and ends the simulation.

(Section III-D). The screen and the radar target simulator stimulated the VUT on the SFT. The distances between the screen and the VUT front camera, as well as between the radar target simulator and the VUT radar sensor, were measured for each vehicle. These known distances were considered in the stimulation so that the on-screen rendering reproduced the exact dimensions and distances that the front camera should perceive. The same procedure was applied to the radar sensor in combination with the radar target simulator.

The simulation method comprised three phases, visualized in Fig. 16:

- In Phase I the VUT accelerated on the SFT to approximately 70 km/h. ACC was set to this speed. When the high beam assist automatically activated the adaptive high beam, the test run proceeded.
- In Phase II the simulation started at time t_0. The target vehicle first appeared at the center of the right lane and remained there for Δt_{start}. The distance between the VUT and the target vehicle was d. The target vehicle then changed lanes with constant speed across all l lanes to the leftmost lane center. The duration per lane change from center to center was Δt_{change}. The target vehicle then remained on the left lane for Δt_{left}.
- In Phase III, the target vehicle moved back with constant speed across all l lanes to the right starting position. It remained there for Δt_{end} before the simulation ended.

On the projection wall, the target vehicle appeared as a bounding box. The position, size, and motion matched the simulation parameters. In parallel, the radar target simulator output the target vehicle as a single point.

2) IMPLEMENTATION

The VUT was accelerated to approximately 70 km/h and held by ACC, as in the previous tests. After the high beam assist activated the adaptive high beam, the on-screen simulation was started.

TABLE 2. Overview of identified parameters varied in Test III.

Category	Parameter	Unit	Range
Scenario	Hold Times Δt_{start}, Δt_{left}, Δt_{end}	s	3
Scenario	Distance VUT–Target Vehicle d	m	20, 25, 30, 50
Scenario	Lane-Change Duration Δt_{change}	s	2, 3, 5
Scenario	Type of Target Vehicle	–	Truck, Passenger Car
Scenario	Number of Lanes l	–	5, 7, 9
Software Aurelion	Retro Light	–	On, Off
Software Aurelion	Ego Vehicle Light in Simulation	–	On, Off
Software Aurelion	Distance Mode d	–	Manual, Constant
Test Bench	Radar Target Simulator	–	On, Off
Test Bench	Screen Brightness	%	50, 100

Because the VUT responses to the simulated target vehicle were not consistently reproducible, we systematically varied several parameters that are expected to influence response stability. However, the resulting configuration space is large and not all parameter combinations could be evaluated within the available test time. The investigated parameters and the tested value ranges are summarized in Table 2.

The hold times Δt_{start}, Δt_{left}, and Δt_{end} were set to 3 s in all tests to provide sufficient time for the VUT to detect the target and classify it as another road user. Since the initial detection was typically successful, these hold times were not varied further.

The distance d between the VUT and the target vehicle was fixed during a run using distance mode *constant* in the Aurelion software. ACC was enabled in the VUT, but it is not perfectly precise. Small deviations from the VUT set speed are possible. For an exactly constant distance, software-side control is preferable. The test bench continuously measures the VUT wheel rotations and thus the traveled distance. The software can adjust the simulated target vehicle position and hold d exactly constant. In manual mode, d depends on the simulated target vehicle speed and the actual VUT speed on the SFT.

Between runs, the distance d was varied from 20 m to 50 m to investigate the influence of target size on the effective spatial resolution of the adaptive high-beam response. At very short distances, the target rapidly moves towards the left or right edge of the projection wall during the lateral maneuver, reducing the number of addressable high-beam segments and thus limiting the diagnostic sensitivity for camera performance. At larger distances, the target appears smaller and allows a finer, more differentiated segment deactivation and

re-activation, enabling a more sensitive assessment. However, excessively large distances may reduce target visibility due to the limited luminance of the display, as the simulated taillights occupy only a small image area.

The lane-change duration Δt_{change} was varied between 2 s and 5 s. Faster lane changes, in combination with the camera frame rate and the recording rate of the projection wall, can cause discrete jumps in the cutoff line to be missed between successive frames. Slower lane changes yield a more gradual transition of the cutoff line and facilitate a finer-grained observation, but become increasingly unrealistic beyond a certain duration.

The target vehicle type alternated between passenger car and truck. This variation was motivated by the assumption that the passenger car might be too small to trigger stable responses, whereas a truck with a larger apparent size could improve detectability and response consistency. However, the truck produced a substantially taller bounding box and, depending on the distance d, parts of the projection could extend beyond the projection wall. While this does not fundamentally prevent the evaluation of the distance between bounding box and cutoff line (which relies primarily on the vertical bounding box boundaries), no improvement in response stability was observed. On the contrary, the truck scenarios tended to yield less consistent results.

The number of lanes l was varied between five and nine. This parameter is closely coupled to the distance d and should be adapted accordingly. For short distances, a high number of lanes provides no benefit because the target reaches the left or right edge of the projection wall after only a few lane changes and may even leave the visible area. The remaining lane changes then mainly increase the overall test duration without adding measurable information. Therefore, l should be selected such that, at the extreme lateral positions (leftmost/rightmost lane), the target bounding box is close to the projection wall edge (potentially with slight clipping), but not far beyond it, to maximize measurable coverage while keeping test time efficient.

The simulation also tested a newly implemented parameter *Retro Light*. With the Retro Light on, the rear reflectors of the target vehicle appeared significantly brighter. The radar target simulator was enabled in some runs and disabled in others, remaining in an idle position. Finally, the screen brightness in front of the VUT front camera was varied between 50 % and 100 %.

3) EVALUATION

Evaluation of the recorded videos was intended to follow Test II (Section III-D.3) with the adaption that the centers of real LED lights were no longer present. Distances would therefore have been computed using the bounding box. Accordingly, C_{L} would have been defined as the distance between the left headlight cutoff line and the leftmost point of the bounding box. C_{R} would have been defined as the distance between the right headlight cutoff line and the rightmost point of the bounding box. Although the evaluation procedure was defined as described above, no statistically conclusive data could be extracted from this test, which is discussed in Section IV-C.

IV. RESULTS AND DISCUSSION

In Test I, a proof of concept was demonstrated. The VUT reacted to detected LED lights and triggered a corresponding vehicle reaction through the adaptive high beam. Thus, the method enables validation of the front camera's *function*. For consistent evaluation a new supporting method was introduced to define the position of the headlight cutoff line. In addition, the experiments revealed that performance depends on both camera calibration and axle geometry, especially the thrust angle. Simulated changes in toe angle resulted in different shadowed segments of the adaptive high beam.

In Test II, the method was extended by dynamically moving the LED lights. The results showed that, in addition to a verification of the *function*, a verification of the *efficiency* is also feasible. Moreover, differences between the vehicles under test became apparent, as varying headlight technologies led to clearly distinguishable reaction patterns.

In Test III, the *efficiency* check of the front camera was transferred to a simulation-based stimulation approach to enable a highly reproducible and systematic procedure. Despite exploring a wide range of simulation parameter combinations, no consistently stable configuration could be achieved. Although the vehicles reacted to the simulated stimuli, the reactions lacked continuity and were therefore not statistically reliable. Under these conditions, a conclusive evaluation was not possible.

A. TEST I: REAL LED LIGHTS - STATIC

Test I first verified the proof of concept. The VUT reacted consistently to each LED light activation and adjusted the adaptive high beam accordingly. Therefore, the developed method at the ViL test bench is suitable for verifying the *function* of a vehicle's front camera.

When calibrating the front camera with deliberately simulated different toe angles of the rear-right wheel, a plausible change in the thrust angle was observed. The correction values output by the DAS3000 calibration system are shown in Fig. 17.

The results show that the correction values for yaw angle increase almost linearly with the size and direction of the inserted gauge block. Starting at 3 cm opposite the driving direction x, via 2 cm opposite the driving direction x and the calibration without a gauge block, up to 2 cm and 3 cm in driving direction x, the correction value of the yaw angle increases continuously.

Pitch and roll hardly changed, as expected, since no related modifications were made.

With the changed yaw angle, the distances D_{L} and D_{R} between the LED light centers and their respective cutoff lines also changed.

Fig. 18 illustrates this with an example frame.

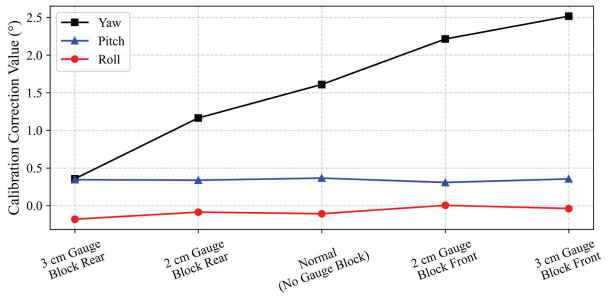

FIGURE 17. Correction value angles output by the DAS3000 after completing a front camera calibration with the respective gauge block to simulate a different toe angle of the rear-right wheel.

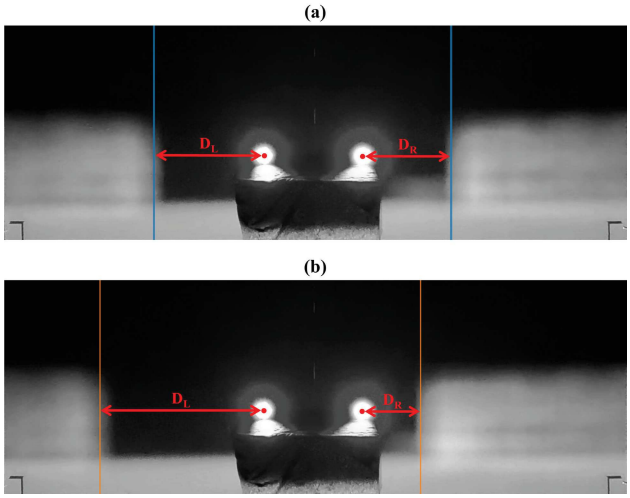

FIGURE 18. Example from the static evaluation in Test I. (a) The blue vertical bands show the detected headlight cutoff lines for Normal (no gauge block), 2 cm gauge block in x, and 3 cm gauge block in x, (b) The orange vertical bands show the detected headlight cutoffs for 2 cm gauge block opposite x and 3 cm gauge block opposite x.

The example frame shows the vehicle reaction for the first of five activations. The vertical bands represent the measured D_L and D_R across all five repetitions. These are not mean values, all values actually lie within these narrow bands. The vehicle reaction is therefore highly consistent with very low scatter. The color-coded areas differ by calibration state: in (a), the blue areas visualize D_L and D_R for calibrations with gauge blocks (2 cm, 3 cm) in driving direction x and without a gauge block, in (b), the orange areas visualize D_L and D_R for calibrations with gauge blocks (2 cm, 3 cm) opposite driving direction x.

Changing from no gauge block to 2 cm opposite x shifts the cutoffs from blue to orange. Accordingly, D_L increases and D_R decreases. The relation between the inserted gauge blocks and the correction value for the yaw angle can explain this behavior.

The camera itself remains mechanically unchanged at all times. The correction values output by the DAS3000 are all positive. Positive correction values indicate a negative thrust angle, which must therefore be compensated in the positive direction. Increasing positive correction values correspond to a more negative thrust angle. As the thrust angle becomes more negative, the camera, which is aligned with the thrust axis, effectively points further to the right in the direction of driving.

A positive correction value indicates that the system recognizes that the camera image should actually capture the scene further to the left in the direction of driving. Since the camera cannot be physically rotated, the perceived object positions are corrected via software. Assuming an object is detected in the image center, a virtual rotation of the camera to the left would cause the perceived object to shift to the right in the image. This simplified thought experiment explains the observed behavior: the more negative the thrust angle, the stronger the perceived rightward shift of objects in the driving direction. Conversely, smaller correction values result in less rightward compensation, causing objects to appear further to the left in the image.

This behavior is also visible in Fig. 18. In (a), the thrust angles are more negative and the correction values are therefore higher, resulting in a stronger rightward shift of the object in the driving direction. The middle area is shadowed. In (b), the thrust angles are more positive, and although the correction values remain positive, they are smaller, leading to a smaller rightward shift. Consequently, the object appears further to the left, and the system shadows the corresponding left area.

The adjustment of the cutoff lines does not occur continuously but in discrete steps. The segmented structure of the adaptive high beam modules in the Škoda Octavia is the cause. Continuous regulation is therefore not possible, only discrete segment changes occur. When OEM-defined thresholds for minimum or maximum distances between the cutoff line and the object are exceeded or fall below, the system shifts to the next segment, causing abrupt changes in distance. In the conducted tests, such a threshold could be identified. The threshold is exceeded between the calibration without a gauge block and the one with a 2 cm gauge block opposite to x, which leads to a visible change in the shadowed segments.

A PTI inspector can immediately visually identify incorrect calibration values or axle geometry using this method. If a target is shadowed centrally, as shown in Fig. 18(a), the camera calibration and axle geometry are likely matching. A significantly incorrect calibration or misaligned geometry can be directly detected through large differences between D_L and D_R. However, it is worth noting that OEMs may define different thresholds, as well as varying numbers and widths of adaptive segments, which can limit generalization. Nonetheless, a critical error can be directly identified if either D_L or D_R is negative, meaning that an LED light center lies within an illuminated region, potentially causing glare for other traffic participants.

B. TEST II: REAL LED LIGHTS - DYNAMIC

In Test II, the method from Test I was extended by dynamically moving the LED lights. The goal was to verify the front camera's *efficiency* when the stimulating objects move

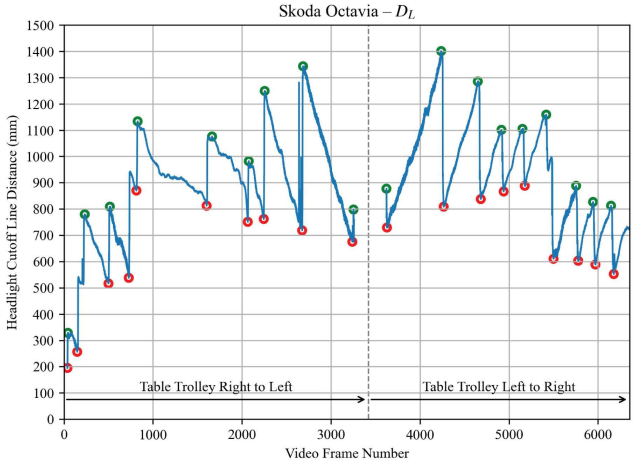

FIGURE 19. Distances D_L with dynamically moved LED lights for the Škoda Octavia. Local minima (red) and local maxima (green) are marked. The dashed line indicates the manually defined midpoint of the captured video frames. Left of the dashed line, the trolley was moved from right to left, and right of the dashed line, it was moved from left to right.

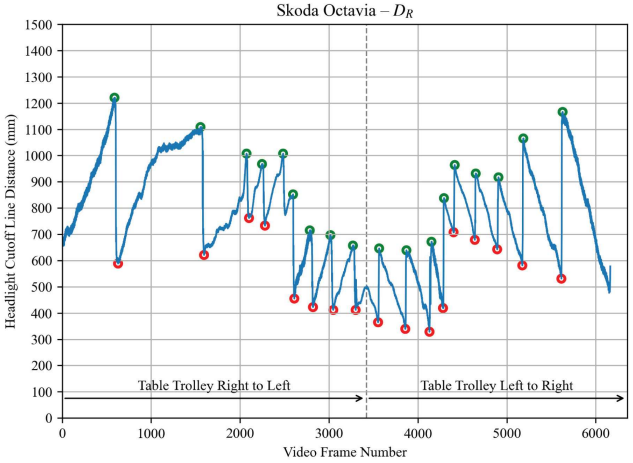

FIGURE 20. Distances D_R with dynamically moved LED lights for the Škoda Octavia. Local minima (red) and local maxima (green) are marked. The dashed line indicates the manually defined midpoint of the captured video frames. Left of the dashed line, the trolley was moved from right to left, and right of the dashed line, it was moved from left to right.

within the field of view. This was demonstrated at the ViL test bench, showing that the method enables not only a *function* check but also a quantitative *efficiency* check. Additionally, an initial automated evaluation of the vehicle's reactions was implemented and applied.

For all examined VUT, it was quantitatively verified that the front camera reacted to the dynamically moving LED lights and adjusted the cutoff lines. However, the quality of reactions differed: the Škoda Octavia showed very consistent and well-measurable behavior, whereas the Volkswagen Passat and Ford Focus results contained some gaps.

For evaluation, D_L and D_R were plotted over the respective video frames. Note that the x-axis counts frames and is therefore only approximately time-equivalent because the trolley did not move at exactly constant speed.

Fig. 19 and 20 show the distances D_L and D_R over the frames. The trolley with the LED lights was moved from right to left and then returned to its original position.

A sawtooth pattern appears. Moving the trolley right-to-left, D_L decreases continuously as the LED "catches up" with the cutoff lines, until the cutoff line jumps to the next segment and the distance increases abruptly. Analogously, during this motion D_R first increases, then drops when the cutoff line jumps. On the return motion, the pattern reverses. This is consistent with segment-wise regulation of the cutoff lines in the Škoda Octavia and is similar to those in the Volkswagen Passat.

Notably, the minima and maxima (red/green) vary rather than being constant. Especially when the trolley is centered in front of the VUT (around one-quarter and three-quarters of the frame count), the minima (red) are largest. This suggests that manufacturer thresholds for segment switching are context-dependent. The object position in the field of view appears to be influential: local minima are of higher minimal distance near the camera center than at the edges, presumably to avoid central glare more robustly.

Importantly, negative distances D_L and D_R should not occur, as that would imply an LED is not shadowed and a traffic participant would be glared at in real driving. This did not occur in our tests. However, the applied evaluation method has methodological limits: around the LED centers, the search for the cutoff is only started once $B_{\text{mean}}(x) < T$ holds, and the search proceeds only outward (left of the left LED, right of the right LED), see Section III-C.3. If a cutoff line lies between the LED light centers, it will not be detected. Such a case would indicate a severely misadjusted vehicle. In practice, a PTI inspector would likely detect such a large deviation visually, rendering a quantitative evaluation unnecessary in that scenario.

The Škoda Octavia and the Volkswagen Passat thus confirm that the developed method at the ViL test bench is, in principle, suitable for a quantitative evaluation of the front camera's *efficiency*.

For the other VUT Ford Focus reactions were different and shown in Fig. 21 and 22.

The Ford Focus regulates the cutoff line continuously and therefore does not use discrete light segments like the Škoda Octavia or Volkswagen Passat. The visible small jumps are thus not caused by segment switching but can be attributed to occasional irregularities in detection or regulation. Overall, the trend of progression is approximately linear.

Compared to the other VUT, the measured distances were significantly larger, mostly exceeding 1000 mm. Due to these greater distances, the cutoff line often extended beyond the projection wall, preventing valid measurements. As a result, the data became sparse, particularly for the right cutoff (Fig. 22). D_R could only be detected when the trolley was positioned at the leftmost side of its range of motion. At all other positions, the right cutoff line extended beyond the projection wall, or the light pattern was irregular.

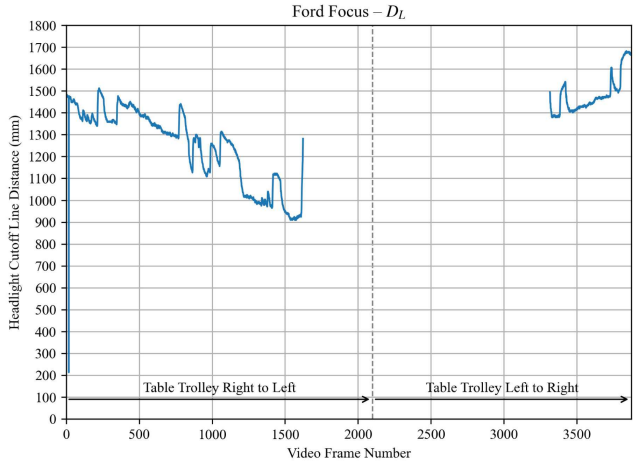

FIGURE 21. Distances D_L with dynamically moved LED lights for the Ford Focus. The dashed line indicates the manually defined midpoint of the captured video frames. Left of the dashed line, the trolley was moved from right to left, and right of the dashed line, it was moved from left to right.

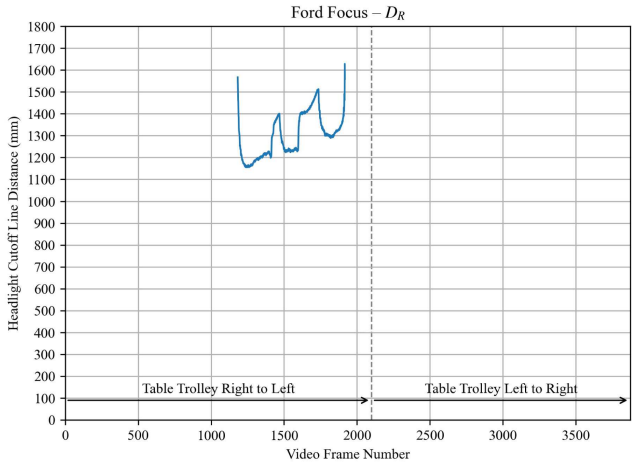

FIGURE 22. Distances D_R with dynamically moved LED lights for the Ford Focus. The dashed line indicates the manually defined midpoint of the captured video frames. Left of the dashed line, the trolley was moved from right to left, and right of the dashed line, it was moved from left to right.

C. TEST III: SIMULATED TARGET VEHICLE - DYNAMIC

In Test III, the *efficiency* check was to be transferred to a simulated environment to enable high reproducibility. However, no statistically significant results could be achieved. Although the variation of parameters listed in Table 2 influenced the outcomes, continuous and consistent vehicle reactions could not be elicited.

In earlier pre-tests, reproducible vehicle reactions had been observed with other VUT, such as a Porsche Taycan, making the cause of the inconsistent behavior in the main test series unclear. While the initial deactivation of high-beam segments in response to the target was typically triggered, the VUT frequently lost the target during the maneuver. In these cases, the system either re-activated full high beam (i.e., illuminated all segments) or switched the high beam off entirely. Both behaviors prevented a meaningful continuation of the run and therefore required aborting the trial, so that the data could not be evaluated. Despite the systematic parameter variations described in III-E.2, the response stability could not be improved to a reproducible level.

Another possible reason could be changes or software updates in dSPACE Aurelion [44] between the pre-tests and the main experimental campaign, which may have reduced the detectability of the simulated environment for the VUTs front camera.

Furthermore, the brightness of the simulation screen may have had a significant influence on triggering the vehicle reaction. As already observed in prior research on high-beam assist behavior [24], excessive screen luminance can increase the perceived ambient illumination and thereby suppress high-beam activation by the high-beam assist. Conversely, if the brightness is too low, the VUT may fail to detect the simulated environment correctly. Accordingly, both overly bright and overly dim display settings can impair the perception pipeline and contribute to unstable or missing reactions.

These observations highlight the sensitivity of deploying the approach on a ViL test bench: even minor changes in the simulation or rendering chain may affect camera perception and thus the resulting vehicle behavior. Consequently, further work is required to identify and control the dominant influencing factors before the proposed method can be applied for robust and reproducible front-camera verification.

D. FURTHER DISCUSSION

Additional limitations and improvement potentials identified in this work are discussed below.

First, in the evaluation, the cutoff line was detected only to the left of the left LED light and to the right of the right LED light. If a cutoff line lies inside this zone, the current method will not detect it. In practice, such a scenario would indicate a severely misadjusted vehicle, which would already be easily and visually noticeable during a PTI. For future work, it could nevertheless be useful to adapt the supporting method to detect inner cutoff lines as well. This is particularly relevant for a potential automation of the evaluation, e.g., if no inspector is present or if the inspector momentarily does not observe the projection while the corresponding segments are deactivated. Conceptually, the approach could be extended by searching for cutoff lines across the full width of the projection wall using a similar detection scheme as in this work, but with an adapted search-window width and an additional assignment step that links each detected cutoff line to the left or right LED (or bounding-box edge). In the nominal case, two cutoff lines are expected (left and right of the stimulated object); then, the leftmost detected cutoff line can be assigned to the left LED and the rightmost to the right LED. If no cutoff line is detected, the evaluation can be skipped for that frame. If three or more cutoff lines are detected, this would indicate an implausible situation for a single stimulated object and may point to disturbances such as reflections or unintended additional objects; this case can be flagged for manual review. A special case arises when only one cutoff line is detected, which may occur if the

second cutoff line lies outside the projection wall (e.g., due to larger tolerances and cutoffs as observed for the Ford Focus). In such cases, the left/right identity can be inferred from the local polarity of the luminance transition: for the left cutoff line, the region immediately left of the cutoff is typically darker and the region immediately right is brighter, whereas for the right cutoff line the polarity is reversed. One practical challenge is that cutoff lines located very close to the LED images can be obscured by the high luminance of the LED region in grayscale recordings. A possible mitigation is to search for the cutoff line at a slightly different vertical offset (above/below the LED region) to avoid saturation artifacts, which, however, requires verifying that the cutoff remains visible at the chosen height. Overall, these extensions are feasible but require further research to robustly handle edge cases and to validate reliable assignment under varying projection and illumination conditions.

Second, in this work, the cutoff line is always detected as a vertical straight line. In some adaptive high beam patterns, cutoff lines can be curved, slanted, or kinked. For this work, creating consistent comparability is acceptable. For other objectives, it may be necessary to capture the true geometry of the cutoff lines. However, even if the cutoff line exhibits a different geometry, the proposed method can still be sufficient for detection. In particular, since only a narrow local region of interest (41 px in width) is analyzed, the global shape of the cutoff line is of minor relevance within this small window and a local linear approximation is generally adequate. A failure case would only be expected if the cutoff line is strongly non-linear within the region of interest, such that no consistent luminance transition is present across the analyzed columns. As illustrated in Fig. 13, the evaluated area is limited and the transition is assessed locally based on short horizontal intensity profiles. If needed for specific patterns, the detection parameters can be adapted systematically, e.g., by reducing the vertical extent of the analysis window to enforce local linearity, decreasing the required number of consecutive pixels/columns indicating a transition, or replacing a fixed threshold with an adaptive or interval-based criterion. Overall, the current approach has proven robust in the experiments conducted and is, in principle, applicable also to non-linear cutoff lines as long as a locally consistent transition is present.

Test I could still be evaluated manually, and the results were individually verified. Starting with Test II, an automated evaluation had to be developed, as manual effort would no longer have been feasible given the large number of frames. The evaluation method developed in this work is not entirely error-free. In some rare cases, the detection of the LED light centers or the cutoff lines may have been inaccurate. However, a quick manual review revealed no frequent or systematic errors. Therefore, no outlier removal was applied. For future improvement of robustness, the evaluation method could be extended to include an automated outlier handling.

A potential influence on the measurements is lateral VUT motion on the SFT. Although the driver tried to avoid lateral movement, small motions cannot be ruled out. Lateral motion would alter the projected headlight pattern and, consequently, the cutoff line position. However, Fig. 18 shows that the detected cutoff lines lie very close together, usually differing by only a few pixels. Given the segmented nature of the adaptive high beam, changes occur in discrete segments, not pixel-wise, these deviations are irrelevant for the tests. Nonetheless, the small deviations in the results may reflect minimal lateral motion of the VUT on the SFT.

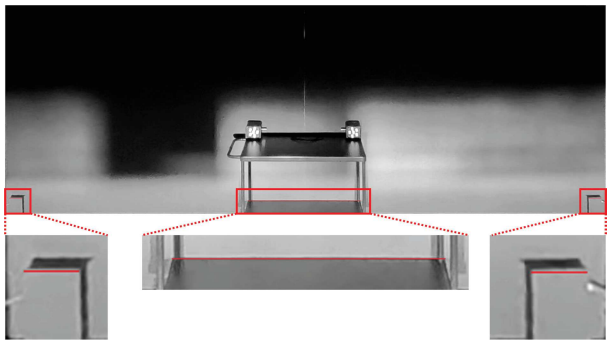

FIGURE 23. Example frame used for validation of the pixel-to-millimeter scaling. Two wall-mounted reference protrusions (left/right) and the table trolley (center) serve as known-width features. The measured pixel width is highlighted in red.

The perspective correction performed well (Section III-C.3). The scaling factors $z_{\text{horizontal}} = 3.61\,\text{mm/px}$ and $z_{\text{vertical}} = 3.68\,\text{mm/px}$ are very close. Relative to the projection wall dimensions (5680 mm width, 2000 mm height), this corresponds to maximum deviations of about 103 mm and 35 mm, i.e., below 2 %. This indicates that the perspective rectification reliably compensated for the distortion. To further validate the rectification and the derived scaling factors, three additional reference widths with known real-world dimensions were selected within a single representative frame. These reference features were chosen because they are distributed across the projection wall (*left*, *center*, and *right*), allowing potential residual non-uniformities over the image width to be captured. For each feature, the width in pixels was measured in the single frame (using Microsoft Paint) and compared against the corresponding ground-truth width. Figure 23 illustrates the selected reference structures: two distinct protrusions mounted directly on the projection wall at the far left and far right, and the table trolley located in the center.

For improved readability, each reference feature is additionally shown as a zoomed-in view, where the measured pixel width is highlighted in red. When measuring the wall-mounted protrusions, care must be taken to avoid shadow edges, as the dark regions can include substantial cast shadows and may bias the apparent feature boundary. For the table-trolley reference, the rearmost visible edge must be used, since this edge lies nearly in the plane of the projection wall and therefore represents the correct width after mapping all measurements to the wall plane. In contrast, using the front edge would systematically overestimate the width due to perspective effects, thereby distorting the validation. The

left and right wall protrusions yielded a deviation of 1.87 mm between the measured and real widths, i.e., the ground-truth width was about 1.5 % larger than the value derived from the example frame. For the table trolley, the accuracy was even better: the computed width was 1064.95 mm compared to a real width of 1070 mm, resulting in an absolute deviation of 5.05 mm, which corresponds to only about 0.5 % relative to the full real width. This comparison constitutes an independent validation of the pixel-to-millimeter conversion derived from the rectified projection-wall dimensions. Consequently, all distance values reported in the following are subject to a systematic scale uncertainty on the order of 0.5 % to 1.5 %.

Overall, one big challenge for independent third parties remains that vehicle manufacturers do not provide interfaces to ADAS systems or environmental sensors. Legally, they are not obliged to do so. Such interfaces would, however, be highly beneficial for developing and standardizing new test methods. Future work should therefore examine which methods are practical without manufacturer-specific knowledge and how to design standardized procedures. It should also be discussed how independent third parties could gain legally secured access to the sensor data relevant for *function* and *efficiency* checks, e.g., via the OBD interface. As indicated by the workflow in this work, the inspection process could be significantly simplified if a standardized interface allowed controlled vehicle state inputs, e.g., by emulating a vehicle speed signal so that the high beam assist can be activated even at standstill. This would enable the proposed front camera inspection without requiring a full ViL setup, thereby dramatically reducing complexity and investment costs. With a clearly defined, standardized data access and input concept, similar simplifications could potentially be realized for further inspections of additional environmental sensors. However, it must be noted that such an approach effectively introduces a dedicated test bench mode: it may bypass parts of the full effect chain from perception to processing and vehicle reaction, which could influence overall validity. Moreover, any external interface providing stimulation inputs introduces potential misuse and manipulation risks; therefore, its design would need to incorporate robust cybersecurity requirements and legally secured access control.

If the aspects of a dedicated test bench mode and cybersecurity can be clarified, an implementation within the current PTI framework could be conceivable. This would, of course, not be realized as a full ViL test bench—which would likely exceed the financial capabilities of most PTI facilities—but rather in an adapted, PTI-compatible form. Current PTI procedures already require certain lighting measurements (e.g., for the low beam) to be performed at a defined inspection bay with a level vehicle standing area. Such a controlled inspection spot could be well suited to implement the workflow proposed in this work, for instance by installing a defined projection wall and target in front of the VUT. The PTI adapter is already connected via OBD to start the inspection software and retrieve procedural guidance; with an additional standardized interface, the high beam assist could be enabled under controlled conditions and a simple dynamic real target in front of the VUT could stimulate the front camera. A short visual check of the vehicle reaction and, where feasible, a basic quantitative evaluation using the cutoff line metric, could then provide a PTI-suitable assessment of the front camera's *function* and *efficiency* within a reasonable time budget. Nevertheless, it must be considered that such an approach would initially cover only the front camera; additional cameras (e.g., side-mirror or rear cameras) and other environmental sensors (radar, lidar) would remain untested unless further procedures are added. Therefore, any introduction into PTI must strictly balance diagnostic benefit against inspection time and cost, and would require clear standardization of test specifications and boundary conditions. In this way, PTI could better address the increasing deployment of environmental sensors driven, among others, by EU Regulation 2019/2144 by enabling their in-use verification over the vehicle lifetime.

V. CONCLUSION

This work investigated a method for verifying vehicle front cameras at a Vehicle-in-the-Loop test bench with respect to the periodic technical inspection criteria *function* and *efficiency*. The approach follows the *Input-Process-Output* principle: The input is a defined visual stimulation of the front camera, the process represents the vehicle's internal signal processing, and the output is evaluated via the camera-driven response of the adaptive high beam system.

Three test series were designed and conducted, accompanied by the development of a supporting method to determine the headlight cutoff line to analyze the resulting data. In **Test I**, static LED light sources were used as stimuli, demonstrating a proof of concept for a reproducible *function* check. The vehicle under test consistently responded to the stimuli by deactivating the corresponding adaptive high beam segments. Additionally, simulated variations of wheel toe, influencing the thrust angle, revealed a direct dependency between the adaptive high beam segmentation and the vehicle geometry. This allows deviations from the nominal calibration state to be visually detected by an inspector, highlighting the importance of accurate camera alignment and axle geometry for safe vehicle operation.

In **Test II**, the approach from Test I was extended using moving LED stimuli to evaluate both *function* and *efficiency*. A supporting method was proposed based on a mathematically consistent definition of the cutoff line as the transition between illuminated and shadowed segments from the adaptive high beam. Distance profiles between the cutoff line and the moving LED centers were analyzed to assess the camera performance. The method successfully quantified the reaction dynamics of the adaptive high beam. It revealed characteristic differences in the technologies, contrasting the segmented system of the Škoda Octavia with the continuously dimming system of the Ford Focus.

In **Test III**, the dynamic stimulation was transferred to a highly reproducible simulation environment for further

TABLE 3. Detailed results of the correction values for different simulated toe angles during front camera calibration (Section III-C.1), as well as the corresponding changes in the positions of the adaptive high beam cutoff lines.

Condition for Camera Calibration with Induced Rear Right Wheel Toe Offset via Gauge Block	Calibration Correction Value Yaw (°)	Calibration Correction Value Pitch (°)	Calibration Correction Value Roll (°)	Distance to Headlight Cutoff Line D_L (px)	Distance to Headlight Cutoff Line D_R (px)	Distance to Headlight Cutoff Line D_L (mm)	Distance to Headlight Cutoff Line D_R (mm)
3 cm Gauge Block in x	2.517	0.355	−0.038	279 280 276 277 278 **mean 278**	224 223 226 223 225 **mean 224**	1007.45 1011.06 996.62 1000.23 1003.84 **mean 1003.84**	808.85 805.24 816.07 805.24 812.46 **mean 809.57**
2 cm Gauge Block in x	2.214	0.308	0.004	278 278 280 280 279 **mean 279**	224 223 223 223 223 **mean 223**	1003.84 1003.84 1011.06 1011.06 1007.45 **mean 1007.45**	808.85 805.24 805.24 805.24 805.24 **mean 805.96**
Normal (No Gauge Block)	1.610	0.366	−0.107	278 277 277 281 280 **mean 279**	222 221 222 221 221 **mean 221**	1003.84 1000.23 1000.23 1014.67 1011.06 **mean 1006.01**	801.63 798.02 801.63 798.02 798.02 **mean 799.46**
2 cm Gauge Block opposite to x	1.165	0.338	−0.086	415 413 412 415 412 **mean 413**	146 147 147 146 147 **mean 147**	1498.54 1491.32 1487.71 1498.54 1487.71 **mean 1492.76**	527.20 530.81 530.81 527.20 530.81 **mean 529.36**
3 cm Gauge Block opposite to x	0.357	0.345	−0.180	414 413 413 413 412 **mean 413**	148 146 146 148 149 **mean 147**	1494.93 1491.32 1491.32 1491.32 1487.71 **mean 1491.32**	534.42 527.20 527.20 534.42 538.03 **mean 532.25**

efficiency analysis. However, statistically significant results could not be achieved despite extensive variations in parameters. Possible causes include software inconsistencies or recent system updates.

Compared to earlier low-cost approaches that relied on direct visual stimuli on a display and evaluated only the *function*, the presented Vehicle-in-the-Loop-based method extends the verification to both periodic technical inspection criteria *function* and *efficiency*. Whereas direct periodic technical inspection implementation is currently infeasible due to the complexity and cost of the Vehicle-in-the-Loop setup, the findings form the foundation for deriving simplified and cost-effective test methods for future periodic technical inspection applications. The proposed concept may also be transferable to other environmental sensors, thereby contributing to the long-term functional safety and reliability of automated driving systems throughout the vehicle's lifecycle.

APPENDIX

See Table 3.

ACKNOWLEDGMENT

The authors would like to thank Maximilian Meyer and Felix Finkler from the KÜS Bundesgeschäftsstelle for their valuable support and assistance during the experimental work. They would like to thank Dr.-Ing. Maximilian Bauder for his valuable advice and expertise for this research. They also used ChatGPT (OpenAI) solely for language editing to improve grammar and readability. No scientific content, data analysis, or results were generated by the AI system. All AI-assisted text was reviewed and verified by them.

REFERENCES

[1] Statista. (20, 2023). *Marktvolumen Für Autonome Fahrzeuge Weltweit in Den Jahren 2023 Und 2024 Und Eine Prognose Bis 2029*. [Online]. Available: https://de.statista.com/statistik/daten/studie/1499808/umfrage/weltweites-marktvolumen-fuer-autonome-fahrzeuge/

[2] McKinsey & Company. (2022). *Marktvolumen Für Autonome Fahrzeuge Weltweit Nach SAE-Level Im Jahr 2022 Und Prognose Bis 2035*. [Online]. Available: https://de.statista.com/statistik/daten/studie/1500515/umfrage/marktvolumen-autonome-fahrzeuge-nach-sae-level/

[3] Bosch. (20, 2015). *Anteil Der in Neuwagen Verbauten Fahrerassistenzsysteme in Deutschland in Den Jahren Von 2015 Bis 2016*. [Online]. Available: https://de-statista-com.thi.idm.oclc.org/statistik/daten/studie/510266/umfrage/anteil-der-in-neuwagen-verbauten-fahrerassistenzsysteme-in-deutschland/

[4] (2019). *Verordnung (EU) 2019/2144 Des Europäischen Parlaments Und Des Rates*. [Online]. Available: https://eur-lex.europa.eu/legal-content/EN/TXT/?uri=CELEX%3A02019R2144-20220905

[5] A. Haider et al., "Modeling and simulation of automotive FMCW RADAR sensor for environmental perception," *IEEE Open J. Intell. Transp. Syst.*, vol. 6, pp. 433–455, 2025, doi: 10.1109/OJITS.2025.3554452.

[6] A. Sharif and D. Marijan, "ReMAV: Reward modeling of autonomous vehicles for finding likely failure events," *IEEE Open J. Intell. Transp. Syst.*, vol. 5, pp. 669–691, 2024, doi: 10.1109/OJITS.2024.3479098.

[7] C. Zhang et al., "Global-mapping-consistency-constrained visual-semantic embedding for interpreting autonomous perception models," *IEEE Open J. Intell. Transp. Syst.*, vol. 5, pp. 393–408, 2024, doi: 10.1109/OJITS.2024.3418552.

[8] S. Genser, S. Muckenhuber, C. Gaisberger, S. Haas, and T. Haid, "Occlusion model—A geometric sensor modeling approach for virtual testing of ADAS/AD functions," *IEEE Open J. Intell. Transp. Syst.*, vol. 4, pp. 439–455, 2023, doi: 10.1109/OJITS.2023.3283618.

[9] C. Stadler, F. Montanari, W. Baron, C. Sippl, and A. Djanatliev, "A credibility assessment approach for scenario-based virtual testing of automated driving functions," *IEEE Open J. Intell. Transp. Syst.*, vol. 3, pp. 45–60, 2022, doi: 10.1109/OJITS.2022.3140493.

[10] A. Stoller et al., "Schlussbericht des Verbundes: ErVast—Einsatz dynamischer Verkehrselemente für die Prüfung automatisierter Fahrfunktionen," Version: 1.1, FSD Fahrzeugsystemdaten GmbH, Dresden, Germany, Tech. Rep., 2022. [Online]. Available: https://doi.org/10.2314/KXP:183073427X

[11] C. Mann, "Untersuchungen zur Prüfung von kamerabasierten Fahrerassistenzsystemen im Rahmen der Hauptuntersuchung," Diplomarbeit, Fakultät Kraftfahrzeugtechnik, Hochschule Zwickau, DEKRA Automobil GmbH, Zwickau, Germany, 2019. Accessed: Mar. 11, 2026. [Online]. Available: https://libdoc.whz.de/opus4/frontdoor/index/index/searchtype/collection/id/16239/start/411/rows/1/docId/12371

[12] (2021). *TÜV Rheinland: Fahrassistenzsysteme Im Langzeitbetrieb Nicht Immer Verlässlich*. [Online]. Available: https://presse.tuv.com/fahrassistenzsysteme-im-langzeitbetrieb-nicht-immer-verlaesslich/

[13] (2014). *Richtlinie 2014/45/eu Des Europäischen Parlaments Und Des Rates*. [Online]. Available: https://eur-lex.europa.eu/legal-content/de/TXT/?uri=CELEX%3A32014L0045

[14] (2012). *Strasenverkehrs-Zulassungs-Ordnung (StVZO)*. [Online]. Available: https://www.gesetze-im-internet.de/stvzo2012/

[15] (2025). *FSD Fahrzeugsystemdaten GmbH, DIE FSD—Zentrale Stelle Stellt Sich VOR*. Accessed: Nov. 28, 2025. [Online]. Available: https://fsd-web.de/

[16] *KÜS Bundesgeschäftsstelle, Mit Sympathie Und Sachverstand: Die KÜS, Das Sind Rund 1.600 Prüfingenieure Und Sachverständige, Die Für Sicherheit Rund Ums Fahrzeug Sorgen*. Accessed: Aug. 14, 2025. [Online]. Available: https://www.kues-fahrzeugueberwachung.de/

[17] (2025). *TÜV SÜD AG, Wir Bieten Weltweite Prüf-, Inspektions-und zertifizierungslösungen an*. [Online]. Available: https://www.tuvsud.com/de-de

[18] (2025). *Willkommen Bei DEKRA*. Accessed: Aug. 14, 2025. [Online]. Available: https://www.dekra.de/de/startseite/

[19] (2025). *GTÜ Gesellschaft Für Technische Überwachung MbH, Amtliche Fahrzeuguntersuchungen: Hauptuntersuchung*. Accessed: Aug. 31, 2025. [Online]. Available: https://www.gtue.de/de/privatkunden/vorgeschriebene-fahrzeuguntersuchungen/hauptuntersuchung-hu

[20] M. Atif, A. Ceccarelli, T. Zoppi, M. Gharib, and A. Bondavalli, "Robust traffic sign recognition against camera failures," *IEEE Open J. Intell. Transp. Syst.*, vol. 3, pp. 709–722, 2022, doi: 10.1109/OJITS.2022.3213183.

[21] F. Secci and A. Ceccarelli, "On failures of RGB cameras and their effects in autonomous driving applications," in *Proc. IEEE 31st Int. Symp. Softw. Rel. Eng. (ISSRE)*, Coimbra, Portugal, Oct. 2020, pp. 13–24.

[22] R. Langer, T. Kubjatko, and H.-G. Schweiger, "Challenges in technical inspection of automated vehicles environmental sensors," in *Proc. EVU 32nd Annu. Congr.*, Kufstein, Austria, 2024, pp. 241–249.

[23] M. Gierl, F. Müller, R. Kristen, P. Nenninger, and E. Sax, "Challenges for periodic technical inspections of intelligent cars," in *Proc. 11th Int. Conf. Adv. Vehicular Syst., Technol. Appl.*, Jul. 2022, pp. 41–46.

[24] R. Langer, M. C. G. Eckert, K. Böhm, D. Paula, and H.-G. Schweiger, "Development of a test method for verifying a vehicle front camera using external stimulation," in *Proc. EVU 31st Annu. Congr.*, Limassol, Cyprus, 2023, pp. 262–270.

[25] R. Langer, M. Bauder, G. T. Mogharia, M. C. G. Eckert, T. Kubjatko, and H.-G. Schweiger, "Testing and validation of the vehicle front camera verification method using external stimulation," *Sensors*, vol. 24, no. 24, p. 8166, Dec. 2024, doi: 10.3390/s24248166.

[26] (2025). *KG, ADAS-Tests Im Rahmen Der Hauptuntersuchung (HU)*. [Online]. Available: https://www.rohde-schwarz.com/de/loesungen/automotive-testing/automotive-radar/adas-hauptuntersuchung/adas-tests-im-rahmen-der-hauptuntersuchung257204.html

[27] (2025). *Werkstatt-und Prüftechnologien Der Zukunft*. [Online]. Available: https://www.maha.de/de/news/werkstatt–und-prueftechnologien-der-zukunft

[28] (2025). *FSD Fahrzeugsystemdaten GmbH, ErVast: Einsatz Dynamischer Verkehrselemente Für Die Prüfung Automatisierter Fahrfunktionen*. [Online]. Available: https://www.ervast-projekt.de/projekt.html

[29] (2025). *Dürr Aktiengesellschaft, X-Proof 360*. [Online]. Available: https://www.durr.com/de/produkte/endmontage/prueftechnik/autonomesfahrenpkw/vehicle-in-the-loop-system-fuer-fahrerassistenzsyssteme

[30] R. Büthorn, H. H. Tadjine, B. Auerbach, and K. Schulze, "Advanced headlight system: 3D high beam," in *Advanced Microsystems for Automotive Applications*, J. Fischer-Wolfarth and G. Meyer, Eds., Heidelberg, Germany: Springer, 2013, pp. 77–88.

[31] *Fachkunde Kraftfahrzeugtechnik*, 30th ed., Verlag Europa-Lehrmittel, Haan, Germany, 2013.

[32] Robert Bosch GmbH. (2024). *Intelligent Headlight Control: Ensures Optimum Illumination of the Road*. [Online]. Available: https://www.bosch-mobility.com/en/solutions/assistance-systems/intelligent-headlight-control/

[33] J. K. Nkrumah, Y. Cai, A. Jafaripournimchahi, H. Wang, and V. A. Atindana, "Highway safety with an intelligent headlight system for improved nighttime driving," *Sensors*, vol. 24, no. 22, p. 7283, Nov. 2024, doi: 10.3390/s24227283.

[34] Deutscher Verkehrssicherheitsrat. (2003). *Unfälle in Der Dunkelheit' Schriftenreihe Verkehrssicherheit 12, 2003*. [Online]. Available: https://www.dvr.de/fileadmin/downloads/Schriftenreihe/Schriftenreihe-Verkehrssicherheit-16.pdf

[35] (2024). *TÜV-Report 2024: Die Häufigsten Mängel*. [Online]. Available: https://www.tuvsud.com/de-de/publikationen/tuev-report/die-haeufigsten-maengel

[36] KBA. (20, 2022). *Anzahl Der Mängel Bei Untersuchungen Von Strasenfahrzeugen in Deutschland Nach Ausgewählter Art Der Mängel in Den Jahren 2022 Und 2023*. [Online]. Available: https://de.statista.com/statistik/daten/studie/5312/umfrage/art-der-maengel-bei-fahrzeuguntersuchungen/

[37] S. Pischinger and U. Seiffert, *Vieweg Handbuch Kraftfahrzeugtechnik*, 9th ed., Wiesbaden, Germany: Springer, 2021.

[38] AUDI AG. (2024). *Matrix LED Headlights*. Accessed: Aug. 28, 2024. [Online]. Available: https://www.audi-technology-portal.de/en/electrics-electronics/lighting-technology/matrix-led-headlights

[39] F. Hoberg. (2025). *Matrix-LED, LED Und Laser: Vorteile, Nachteile, Umrüstun*. Aug. 21, 2025. [Online]. Available: https://www.mobile.de/magazin/artikel/matrix-led-licht-technik-49222

[40] L. Möckel. (2025). *Scheinwerfereinstellung: Schon Fünf Millimeter Machen Den Unterschied!*. Accessed: Aug. 14, 2025. [Online]. Available: https://schaden.news/de/article/link/41014/hella-gutmann-scheinwerfereinstellung

[41] (2025). *KÜS Bundesgeschäftsstelle, KÜS Drive—Dynamic Roadworthiness Inspection for Vehicles*. [Online]. Available: https://kues-drive.de/

[42] T. Tentrup, P. Schuler, S. Schuler, T. Auer, and F. Mai, "Wirkprüfungen dynamischer automatisierter bzw. autonomer sicherheitsrelevanter Fahrfunktionen von Kraftfahrzeugen im Rahmen der regelmäigen Hauptuntersuchung," in *Proc. Fachtagung Mechatronik 2022*, T. Bertram, B. Corves, K. Janschek, and S. Rinderknecht, Eds., Dresden, Germany, Mar. 2022. [Online]. Available: https://doi.org/10.26083/tuprints-00020963 and https://tuprints.ulb.tu-darmstadt.de/entities/publication/e0e88644-75f6-49da-a157-30e20ace509c

[43] T. Tentrup, P. Schuler, S. Schuler, and T. Auer, "ADAS Wirkprüfungen zugelassener Kraftfahrzeuge in einer Prüflinie basierend auf dem ViL-Testkonzept: Motivation, Voraussetzungen und Ergebnisse," in *Proc. Mechatroniktagung 2024*, Dresden, Germany, Mar. 2024. [Online]. Available: https://www.vdi-mechatroniktagung.rwth-aachen.de/global/show_document.asp?id=aaaaaaaacjcayqj

[44] (2025). *AURELION: Sensorrealistische Simulation Für ADAS/AD in Echtzeit*. Accessed: Jun. 24, 2025. [Online]. Available: https://www.dspace.com/de/gmb/home/products/sw/experimentandvisualization/aurelion/sensor-realistic/sim.cfm

[45] (2025). *Simulation und Validierung Ihrer Innovationen*. [Online]. Available: https://www.dspace.com/de/gmb/home.cfm

[46] P. Schuler, S. Schuler, T. Tentrup, and T. Auer, "Offenlegungsschrift: Verfahren zur Prüfung der Abstrahlcharakteristik des Lichts eines Kraftfahrzeugs," DE Patent 102 022 102 328 A1, Feb. 1, 2022.

[47] *Straßenfahrzeuge/-Fahrzeugdynamik Und Fahrverhalte/-Begriffe*, Standard ISO 8855:2013-11, 2011.

[48] Robert Bosch GmbH, *Kraftfahrtechnisches Taschenbuch*. Wiesbaden, Germany: Springer, 2024, pp. 1310–1390.

[49] M. Jonas, "Neue Ansätze zur Umsetzung und Durchführung von Kalibrierumfängen bei der Pkw-Inbetriebnahme," Ph.D. thesis, Universität des Saarlandes, Saarbrücken, Saarbrücken, Germany, 2019. [Online]. Available: https://publikationen.sulb.uni-saarland.de/handle/20.500.11880/29333

[50] F. Hirsch. (2016). *Fahrassistenzsysteme Teil 4—Warum Radar Und Kamera Kalibrieren?*. [Online]. Available: https://www.auto-hirsch.eu/2016/10/fahrassistenzsysteme-teil-4-warum-radar-und-kamera-kalibrieren/

[51] Tesla. (2026). *Tesla Vision-Update: Ersatz Von Ultraschallsensoren Durch Tesla Vision*. [Online]. Available: https://www.tesla.com/de/de/support/transitioning-tesla-vision

[52] Robert Bosch GmbH. *DAS 3000 S20: Universelle Computergesteuerte Kalibrier-und Justagevorrichtung*. Accessed: Aug. 22, 2025. [Online]. Available: https://www.boschaftermarket.com/de/de/werkstattausruestung/pruefgeraete/fahrerassistenzsysteme/das-3000-s20/

[53] GoPro. *HERO11 Black*. Accessed: Aug. 22, 2025. [Online]. Available: https://gopro.com/de/de/shop/cameras/heo11-black/CHDHX-111-master.html?srsltid=AfmBOooDSUSzwyZDxy56OlqqKpwavRLLvw,/J44cZ1Qw8crzKSs2pKM-C

[54] (2025). *UKing 2er 6 × 18W RGBWA+UV Akku Led Par Scheinwerfer Wiederaufladbarem Disco Licht Bühnenlicht 9600mAh Batterie Mit Drahtlose Fernbedienung/DMX/APP/2.4 GHZ Für Hochzeit DJ- Versand, Schwarz, (ZQ01430)*. [Online]. Available: https://www.amazon.de/UKing-scheinwerfer-Wiederaufladbarem-B%C3%BChnenlicht-Fernbedienung/dp/B0C5T751JV

[55] Robert Bosch GmbH. (2025). *Quick Start*. [Online]. Available: https://help.boschdiagnostics.com/DAS3000/#/home/62654/de/default

[56] (2016). *Publications Office of the European Union, Regulation No 48 of the Economic Commission for Europe of the United Nations (UNECE)—Uniform Provisions Concerning the Approval of Vehicles With Regard to the Installation of Lighting and Light-Signalling Devices [2016/1723]*. Accessed: Feb. 11, 2026. [Online]. Available: https://eur-lex.europa.eu/legal-content/EN/ALL/?uri=CELEX%3A

ROBIN LANGER received the B.Eng. degree in automotive engineering from Technische Hochschule Ingolstadt (THI), Germany, in 2017, and the M.Sc. degree in mechanical engineering from the Friedrich-Alexander University of Erlangen–Nuremberg (FAU), Germany, in 2020. He is currently pursuing the Ph.D. degree with THI, focusing on testing and verification of environmental perception systems in automated vehicles.

Since 2020, he has been a Research Associate with the Institute of Electric, Connected and Secure Mobility (C-ECOS), CARISSMA, and the Center of Automotive Research on Integrated Safety Systems and Measurement Area, THI. In 2025, he became a Research Team Leader in accident analysis and periodic technical inspection. His research interests include vehicle sensor verification, functional safety, and the future of periodic technical inspection (PTI) for automated driving systems.

THOMAS TENTRUP was born in Marburg in 1957. He received the Dip.-Phys. and Ph.D. degrees in physics from the Faculty of Theoretical Physics, University of Saarland at Saarbrücken, in 1985 and 1990, respectively, in the workgroup of Prof. Rolf Siems. In 1990, the company Dürr Assembly Products (Püttlingen), where he became the Leader of the Department of Product Management and Development with the task to develop new innovative test rigs for the end of line of automotive assembly plants producing passenger cars and commercial vehicles (trucks). Together with his customer VOLVO, he received the worldwide "Ford Technology Award 2008" for "Perfect Steering Wheel Alignment." Since 2015, he has been a Lecturer with the University of Luxemburg for bachelor's and master's students of engineering. In 2020, he changed to the vehicle inspection organization KÜS as the "Director of Research and Development" responsible for the research project to develop and validate the technical possibilities for ADAS effect testing.

HANS-GEORG SCHWEIGER (Member, IEEE) was born in Ingolstadt in 1977. He received the Dipl.-Chem. degree in chemistry from the University of Regensburg, Germany, in 2002, the Ph.D. degree in electrochemistry from the Workgroup of Prof. Heiner J. Gores, University of Regensburg, and the Dr.rer.nat. degree in chemistry from the University of Regensburg in 2004. He joined EVA Fahrzeugtechnik GmbH (Munich) as a Development Engineer in HEV energy storage systems in 2005. In this position, he was appointed as an Engineering Consultant to BMW AG, Munich, Germany. In January 2007, he joined the HEV Department, Continental AG, Berlin, Germany. In this company, he worked as an Expert for lithium-ion batteries. In 2008, he was appointed as a Project Leader in energy storage systems at Continental AG. In this position, he was leading a series of development projects for HEV and EV battery systems and one basic research project for the development of 5-V lithium-ion cells. He was also a part-time Lecturer in electrochemical energy storage systems with the Technical University of Berlin from 2009 to 2011. He was appointed as a Professor in automotive electronics and electric mobility with Technische Hochschule Ingolstadt in 2011. He founded the research group "Safe Electromobility." In 2020, this research group was transformed into the CARISSMA Institute of Electric, Connected and Secure Mobility, where he has been the Head. The primary field of his group are energy storage systems for automotive applications, the safety of electric vehicles, and accident forensics. His workgroup of about 20 co-workers is working on industry and government-financed research projects in the field of automotive energy storage systems. He is also the Director of study programs in the field of electric engineering and electric mobility. He is the author/coauthor of more than 50 research articles and he holds 20 patents. He is a member of VDE and VHB.